Measuring Total Filtration Efficiency of Surgical and Community Face Masks: Impact of Mask Design Features

Silvia Chiera, Alessandro Cristoforetti, Luca Benedetti, Luca Borro, Lorenzo Mazzei, Giandomenico Nollo, Alessio Bucciarelli, and Francesco Tessarolo

***Abstract*— Surgical and community face masks are used worldwide to reduce the transmission of respiratory infections in indoor environments. Performance parameters for these loose-fitting devices are mainly focused on material filtering efficiency, while, differently from face respirators, there are no standard methods for measuring the fraction of air leaking at the face seal. This study quantifies the total filtration efficiency (TFE), a parameter based both on filter efficiency and air leakage, of 50 face mask models with the aim of understanding the role of several mask design features on TFE performance. An instrumented head form equipped with sensors for measuring volumetric airflow and differential pressure was used to simulate the air exhalation from the mouth of a person wearing a face mask. A response surface method (RSM) was used to model the TFE experimental data. Results showed that TFE values ranged over a wide interval (from 5% to 73%), with better values at higher flow rates. A significant positive correlation was found between TFE and filter breathability. The presence of a nosepiece (NP) showed to increase the TFE on average from 4% to 6%, according to the flow rate. Significant improvements were associated only to nosepieces incorporating a metallic wire. The RSM model evidenced that the increase in the number of the filter layers and the use of a meltblown layer result in higher TFE only when a nosepiece is in place. Differently, the benefit of the nosepiece is less marked for masks made of highly breathable filters. To improve overall mask performance, the design of loose-fitting face masks should carefully compromise between breathability and filtration efficiency of the filter materials. The addition of a metallic nosepiece helps improving the TFE by limiting the air leaking at the face seal.**

***Index Terms*— Breathability, COVID-19, differential pressure (DP), face masks, face seal, filtration efficiency (FE), mask design, nosepiece (NP), response surface method (RSM), SARS-CoV-2.**

I. Introduction

THE main route of transmission of SARS-CoV-2 is through inhalation in the upper airways of the aerosols and saliva's droplets generated by respiration, sneezing, and coughing [1], [2], while contact with contaminated surfaces plays a minor role [3], [4]. The use of face masks to cover mouth and nose consequently proved to be among the most effective tools for limiting the spread of SARS-CoV-2 [5]. Recent studies confirmed that the pandemic could be significantly limited by the correct and widespread use of a face mask among the population [2], [6] with particular attention to the correct use and fitting of the masks [7]. Based on these findings, specific recommendations and regulations for the population about face mask use were enforced in many countries [8], [9]. Because of the sudden increase in demand for face masks and the resulting failure of the supply chain [10], new products entered the market exploring alternative systems and materials for protecting the nose and the mouth from potentially SARS-CoV-2 contaminated droplets and aerosol [11]. To create a distinction from medically certified devices (usually identified as "medical" or "surgical" masks), new terms like "homemade masks" [12], [13] or "community masks (CMs)" [14] were adopted for all face mask products that were not meeting the performance and safety standards of medical masks or were not tested for.

In the rapidly evolving context of the COVID-19 pandemic, the World Health Organization published an interim guidance [15] underlying that filtration efficiency (FE), breathability, and face fit are essential characteristics to be considered for all type of face mask in order to guarantee their safety and efficacy.

Unfortunately, the European Standard EN 14683:2019 [16] for surgical mask (SM) and the American Society for Testing and Materials (ASTM) standard for medical masks [17] indicate minimal requirements for bacterial filtration efficiency

Manuscript received 14 October 2022; revised 20 February 2023; accepted 26 February 2023. Date of publication 15 March 2023; date of current version 24 March 2023. This work was supported by the "Laboratorio Associato COrona VIrus Disease (COVID)-19 (LASS) Project" of the University of Trento through internal grant "Bando interno 2020 Università di Trento COVID 19." The work of Francesco Tessarolo was supported by the European Union—Fondo Sociale Europeo Recovery Assistance for Cohesion and the Territories of the European Union (FSE-REACT-EU), Programma Operativo Nazionale (PON) Research and Innovation 2014–2020, under Grant DM 1062/2021. The work of Alessio Bucciarelli was supported by Istituto di Ricovero e Cura a Carattere Scientifico (IRCCS) Istituto Ortopedico Rizzoli (Ricerca Corrente). The Associate Editor coordinating the review process was Dr. Priya Ranjan Muduli. *(Silvia Chiera and Alessandro Cristoforetti are co-first authors.) (Corresponding author: Francesco Tessarolo.)*

Silvia Chiera, Luca Benedetti, Giandomenico Nollo, and Francesco Tessarolo are with the Department of Industrial Engineering, University of Trento, 38123 Trento, Italy (e-mail: silvia.chiera@unitn.it; luca.benedetti@unitn.it; giandomenico.nollo@unitn.it; francesco.tessarolo@unitn.it).

Alessandro Cristoforetti is with the Department of Cellular, Computational and Integrative Biology (CIBIO), University of Trento, 38123 Trento, Italy, and also with the Department of Information Engineering and Computer Science (DISI), University of Trento, 38123 Trento, Italy (e-mail: alessandro.cristoforetti@unitn.it).

Luca Borro is with the Imaging Department/3DLaboratory, Bambino Gesù Children's Hospital, 00146 Rome, Italy (e-mail: luca.borro@opbg.net).

Lorenzo Mazzei is with Ergon Research, 50127 Florence, Italy (e-mail: lorenzo.mazzei@ergonresearch.it).

Alessio Bucciarelli is with the Laboratorio RAMSES, IRCCS Istituto Ortopedico Rizzoli, 40136 Bologna, Italy (e-mail: alessio.bucciarelli@ior.it).

This article has supplementary downloadable material available at https://doi.org/10.1109/TIM.2023.3257326, provided by the authors.

Digital Object Identifier 10.1109/TIM.2023.3257326

(BFE) and differential pressure (DP) but do not provide any methods or equipment to assess the fit on user's face or to quantify the air leaking at the face seal.

Regarding the performance standards of CMs, at present, no mandatory regulation exists, while only a discretionary guide to minimal requirements has been made available by the European Committee for Standardization [14]. ASTM has recently provided a framework for the specifications of barrier face covering performance [18]. However, the document recognizes that no accepted methodologies were defined to measure total filtration efficiency (TFE) from loose-fitting face masks and face coverings despite recent studies have demonstrated the relation of mask design features and fitting with air leakage and overall filtration performance [19], [20], [21], [22].

The quantification of the FE of surgical and community face masks should be based on the analysis of the two pathways for the exhaled air: leakage through the face seal and flow through the filter [23]. These combined effects involve complex airflow phenomena, and, while during the process of inhalation the DP facilitate the sealing of a reasonably well-fit mask [24], it is during exhalation that the increased inner pressure pushes the mask away from the face, inducing higher perimetral leakage [25], [26]. The perfect mask seal for loosely fitting masks, such as SM and CM, is only ideal, and significant leakage at the face seal has been reported in the literature for a range of mask models by several authors [27], [28], [29]. Apart from mask design and material characteristics, leakage at the face seal can be affected by a number of other factors and is highly user-dependent. In fact, facial size and anthropometric features were shown to have an impact on fit and leakage [30], and variability in user compliance with the indications for use in donning a face mask was shown to dramatically modify the fraction of air leaking at the mask perimeter [27].

Differently from inward protection, which can be determined by established standard mask fit tests, the flow physics of outward protection is a far less studied phenomenon, both experimentally and computationally [31], [32], [33]. Person-to-person variability and the effect of the expiratory particle size on FE are further aspects in need of scrutiny [34]. As shown by prepandemic studies, given the relevant number of particles that can pass through the face seal, establishing an optimal fit should be of upper importance during mask development, to minimize face seal leakage [23]. To complete the characterization of the overall efficacy of SM and CM, it is then urgent to integrate the FE of the filtering material with the quantification of the fraction of exhaled air leaking at the face seal. Additionally, the accurate evaluation of protection efficiency of face masks should direct improvements to their design and inform guidelines about their usage [24]. A large interest remains, even after the pandemic peak, in educating the population about the correct use of personal protective equipment for preventing respiratory infections [21], spurring the research on simple performance metrics to predict the impact of materials and designs on mask efficiency [35].

Several studies evidenced the importance of evaluating the airflow leaking from face masks since the unfiltered air exhaled by an infected person can play a critical role in virus transmission [20]. However, most of the experiments performed to study the ability of face masks at containing the viral spread relied on qualitative tests, showing leak flow preferential direction, droplet projection distance, or aerosol density distribution [6], [20], [23], [29], [36], but without providing numbers on the fraction of air leaking at the face seal. More recently, the fraction of the respiratory droplets and aerosol blocked by cloth masks was measured by Lindsley et al. [35] and coworkers, using a setup that included a realistic head form, a large aerosol chamber, and a multistage aerosol impactor. Further experimental studies, in vivo, in vitro using manikins, and in silico, evidenced the importance of considering material breathability combined with mask design factors, revealing the role of the fit of the mask in impacting the filtering efficiency [30], [37], [38]. Ipaki et al. [30] proved how face anthropometry can influence the fitting, suggesting a redesigning of face mask parameters by adjusting leakage critical points with a paper prototype fit on the user's face. Wang et al. [37] and Solano et al. [38] studied how leakages were linked to a wide variety of facial characteristics and mask designs using a 3-D-scanning face model. Further studies on face mask fitting were also conducted with finite-element analysis and aimed at studying the contact pressure between mask and facial anatomy [39]. Additive manufacturing (AM) was investigated in silico by Carr et al. [19] as a mean to optimize fitting and reduce leakage, obtaining an effective sealing only by filling the gap between the mask and the face with an adaptable gasket added to the rigid AM materials. Breathability, dependent on the mask filtering material characteristics, also emerged as an important parameter influencing mask FE via its strong causal relationship with leakage [27], [40].

The accuracy and reproducibility of both leakage and breathability measurements need to be investigated further in relation to the experimental errors [41], [42]. Since there is a lack of information on how the intrinsic variability among mask samples could affect measurement uncertainty, replicated measurements appear the most reliable experimental approach to estimate the confidence of any newly introduced mask performance parameter. This strategy has been pursued in previous pilot studies by Chiera et al. [27], [43] for measuring leakage and the TFE, mainly focusing on the influence of wearing styles and mask breathability on the overall mask performance.

This study is aimed at applying a recently developed method to quantify the outward TFE on a wide range of SM and CM, not only to extend the evaluation of filtration performance on a more comprehensive number of face covering products and grabbing a clearer view about TFE measurement uncertainty and variability, but also with the goal of understanding the role of several mask design parameters and filter properties on TFE, providing evidence-based indications for the design and fabrication of more efficient face masks.

II. Materials and Methods

In this study, to determine the mask TFE, we exploited the method for the quantification of the leakage fraction of face masks we recently developed in [27]. The method is based on an instrumented head form equipped with sensors

for measuring volumetric airflow and DP. Details of the test rig, the theoretical model, and the data analysis process are detailed in [27] and summarized here.

A. Theoretical Model

In real conditions, where the face fit of the mask is not perfect, the total airflow $Q_{\text{I tot}}$ exhaled by the mouth splits into two components, $Q_{\text{I mask}}$ passing through the mask filter and the $Q_{\text{I leak}}$ leaking through the mask boundaries

$$Q_{\text{I tot}} = Q_{\text{I mask}} + Q_{\text{I leak}}. \tag{1}$$

The resistance created by the face mask materials and design to the exhaled airflow determines the DP ΔP_{I} between the inside of the mask and the external environment, which is the common driver for both $Q_{\text{I mask}}$ and $Q_{\text{I leak}}$. This DP is also linked to the breathability of the mask since lower ΔP_{I} values facilitate the mask user's breathing. By definition, $Q_{\text{I mask}}$ is only determined by the resistance $R_{\text{I mask}}$ of the mask filter. According to Darcy's law [44], the volumetric flow rate of a fluid with a viscosity μ through the porous medium having a cross-sectional area A, a thickness L, and a permeability k is proportional to pressure drop applied across the porous medium [45]. This allows modeling the flux through the mask material as

$$\Delta P_{\text{I}} = Q_{\text{I mask}} \cdot R_{\text{I mask}} \tag{2}$$

where $R_{\text{I mask}}$ is related to the filter permeation characteristics as follows:

$$R_{\text{I mask}} = \mu \text{L/kA}. \tag{3}$$

Differently from $Q_{\text{I mask}}$, $Q_{\text{I leak}}$ cannot be simply modeled or calculated since the resistance of the airflow escaping from the mask seal is related both to flow velocity and turbulence, and the size and shape of the openings at the face seal interface.

In order to obtain separate measurements for the components $Q_{\text{I mask}}$ and $Q_{\text{I leak}}$, we devised a two-phase experimental protocol which included measurements in the ideal experimental condition where no air leak was present (perfect mask fit to the face). This condition is described by a flux model where the total airflow is represented only by the flow passing through the mask $Q_{\text{II mask}}$, which can be related to the mask resistance $R_{\text{II mask}}$ and the DP ΔP_{II} measured in ideal condition by the following equation, similar to (2):

$$\Delta P_{\text{II}} = Q_{\text{II mask}} \cdot R_{\text{II mask}}. \tag{4}$$

B. Experimental Setup

The TFE calculation was based on the measurement of the $Q_{\text{I mask}}$ fraction of the exhaled air performed with an experimental setup based on a polylactic acid dummy head. A comprehensive view of the experimental setup is presented in Fig. 1. The dummy head was 3-D-printed according to the dimensional characteristics of the medium-sized head, as specified by the standard ISO 16900-5 [46]. The porosity of the surface was reduced by sandpaper and epoxy resin finishing.

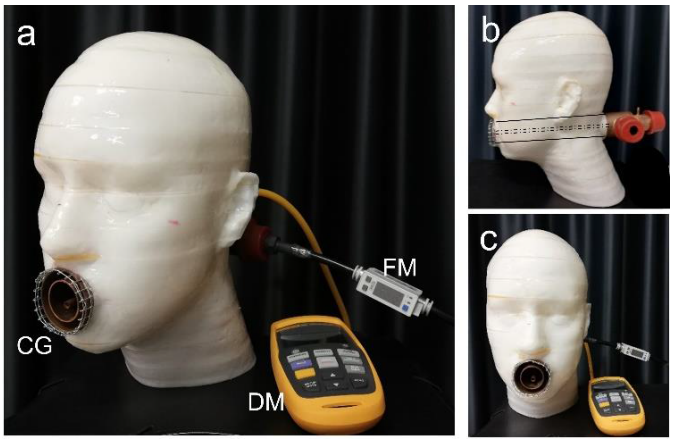

Fig. 1. Experimental setup for the measurement of face masks leak fraction: (a) dummy head instrumented with the pipe system, the outlet CG, the connected DM, and the compressed air supply equipped with the FM; (b) side view, indicating the inner piping connecting the mouth opening with the airflow inlet and the DP manometer; and (c) front view of the setup. Reprinted with permission from [43].

The head form was then instrumented with a pipe system which conveyed a controlled airflow from a compressed air supply to the mouth region, as specified in part 8.9 of the EN 149:2009 standard [47]. The outlet of a 42-mm-diameter tube, devoted to simulating air inhalation (not used in this study), was present at the mouth region. Air exhalation was instead simulated by an inner concentric tube of 28 mm in diameter. The pressure at the center of the mouth opening was sampled by using a differential manometer (DM), referred to environmental pressure, connected to the mouth by a third smaller tube (6 mm in diameter). Exhalation was mimicked by a constant airflow generated by the compressed air supply through the 28-mm tube, measured by a dedicated flowmeter (FM). A circular grid (CG) placed on the mouth opening prevented direct contact between the outlet and the mask surface, allowing a homogeneous spread of the flow outside the mouth even when the ear loops tightly pressed the mask on the dummy head.

The airflow values specified for testing face respirators according to the standards [17], and typically generated during speech [49], were reproduced in this study by generating an airflow rate between 30 and 160 L/min. The airflow rate exiting the dummy head in steady-state conditions was measured by a digital flow sensor (Digital Flow Switch PFM7, SMC Corporation, Tokyo, Japan) claiming an accuracy of 3% of the read value [+1 least significant digit (LSD)] and a resolution of 1 L/min for air at 25 °C in the 2–200-L/min measuring range. The DP ΔP, occurring between the dummy head mouth opening and the exterior environment, was measured by a DM (Fluke 992, Fluke Corporation, Everett, WA, USA), claiming an accuracy of 1% of the read value (+1 LSD) and a resolution of 1 Pa in the 1–4000-Pa measuring range. Both the FM and the DM were calibrated from the manufacturer, and study measurements were collected within one year from calibration date. Deviations from the volumetric airflow measurement due to shift of environmental temperature (21 ± 2) °C from nominal working temperature and possible differences in pressures occurring at different experimental phases were negligible (<0.1%).

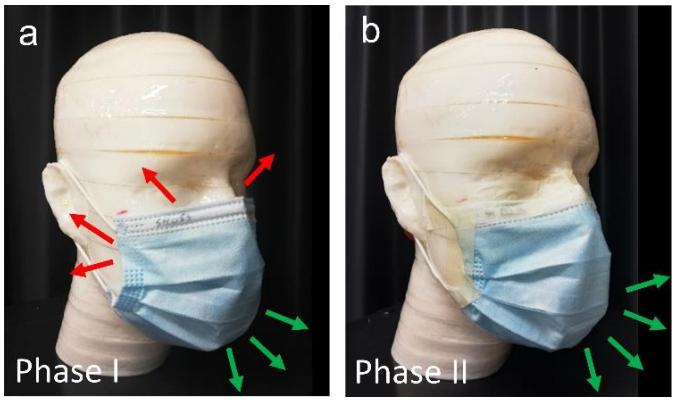

Fig. 2. Face mask mounted on the head form during the two different phases of the experimental protocol: (a) phase I of the experiment and (b) phase II of the experiment. Note the adhesive tape used for sealing the gap at face–mask interface during phase II of the experiment. The superimposed arrows conceptualize the exhaled airflow passing through the leaks (red arrows) and through the mask (green arrows). Reprinted with permission from [43].

C. Experimental Protocol

The experiment consisted of two phases corresponding to different modalities of applying the mask to the face dummy (Fig. 2). Their comparison allowed separating and quantifying the exhaled airflow components passing through the mask filter and leaking through the boundary.

The first phase (Phase I) emulated the real situation of wearing a mask, where leaks are present and no extra means were applied to set the mask in place [Fig. 2(a)]. The positioning of the tested masks on the dummy head followed manufacturer's instruction for use (IFU), covering both nose and mouth, hanging the ear laces at their intended position, and applying fingers pressure to conform the mask border as much as possible to the dummy head surface. Whenever present, the nosepiece (NP) was also carefully adapted to the nose ridge profile to optimize the mask seal.

With the mask properly positioned, constant airflow rates $Q_{\mathrm{I\,tot}}$ were generated from the air supply, and when reaching a steady-state condition (5 s after reading the expected airflow rate on the FM), the corresponding values of DP ΔP_{I} were collected on the DM. The procedure was performed for $Q_{\mathrm{I\,tot}}$ equal to 30, 90, and 160 L/min, as they were considered representatives for low, medium, and high flow rates during real breathing conditions.

The second phase (Phase II) of the experiment mimicked the ideal situation of a perfect mask fit, where no leak is present, and the entirety of the exhaled airflow passes through the mask filter. To achieve this condition, after the mask was fit on the dummy head according to the same procedure of Phase I, the mask boundaries were hermetically sealed on the dummy surface using adhesive tape (paper masking tape, 25 mm width, Tesa[1] Masking Economy, Tesa SE, Hamburg, Germany), avoiding in this way any air leakage [Fig. 2(b)]. The tape was applied on the peripheral welded areas of the mask that do not contribute to air filtering, ensuring the absence of any residual gap by visual inspection of tape adherence both before and after each measurement. Several steady-state airflow rates, indicated as $Q_{\mathrm{II\,mask}}$, were generated in these experimental conditions, and the corresponding set of DP measurements, indicated as ΔP_{II}, was collected. In Phase II, $Q_{\mathrm{II\,mask}}$ varied from 30 to 160 L/min, at increments of 10 L/min.

[1]Trademarked.

D. Data Analysis

The measurements of $Q_{\mathrm{I\,tot}}$ and ΔP_{I} obtained in the realistic conditions of Phase I do not allow separating the fraction of leaked airflow from the total airflow in (1) since the separate contributions of filter ($R_{\mathrm{I\,mask}}$) and seal to overall mask resistance are unknown. However, in the experimental conditions of Phase II, values of $R_{\mathrm{II\,mask}}$ were determined by using (4) for 14 measurements of ΔP_{II} and $Q_{\mathrm{II\,mask}}$ (every 10 L/min in the airflow range from 30 to 160 L/min). To take into account minor variations of mask resistance at different air pressure, the analytical profile of $R_{\mathrm{II\,mask}}$ as a function of ΔP_{II} was modeled by fitting a first-order polynomial curve on the calculated $R_{\mathrm{II\,mask}}$ data, as previously detailed in [43]. Based on the linear regression model, the values of $R_{\mathrm{I\,mask}}$ were predicted for the ΔP_{I} corresponding to $Q_{\mathrm{I\,tot}}$ equal to 30, 90, and 160 L/min. The predicted $R_{\mathrm{I\,mask}}$ values were then used in (2) to compute the values of $Q_{\mathrm{I\,mask}}$ corresponding to ΔP_{I}. Then, the mask fraction F_{mask}, in agreement with [27], was defined as the fraction of the exhaled airflow passing through the mask filter and was calculated according to the following equation:

$$F_{\mathrm{mask}} = \frac{Q_{\mathrm{I\,mask}}}{Q_{\mathrm{I\,tot}}} = \frac{\Delta P_{\mathrm{I}}}{R_{\mathrm{I\,mask}} \cdot Q_{\mathrm{I\,tot}}}. \tag{5}$$

To characterize the outward TFE of a mask, we finally took into consideration the BFE of the mask filter measured according to the method specified in Annex B of standard EN 14683:2019 [16] using the test rig previously described in [11] and characterized in [42]. Finally, the mask TFE was obtained according to the following equation:

$$\mathrm{TFE} = F_{\mathrm{mask}} \cdot \mathrm{BFE} = \frac{\Delta P_{\mathrm{I}}}{R_{\mathrm{I\,mask}} \cdot Q_{\mathrm{I\,tot}}} \cdot \mathrm{BFE}. \tag{6}$$

E. Face Masks Tested in This Study

The experimental protocol was applied to 50 different face mask models (Fig. A, supplementary material) representative for a range of masks available in the market. The considered models included masks made of woven and/or nonwoven materials, in a range of different designs, varying by the number of filter layers, the filter materials, the filter structure, and the retention system. Specifications of each mask are reported in Table I, including the values of breathability (DP, expressed in Pa/cm^2) and BFE (expressed as %) obtained at our laboratory according, respectively, to the methods defined in Annexes B and C of standard EN 14683:2019 [16], using the equipment previously presented in [11]. Information about the presence of a nosepiece is also listed.

Based on the DP and BFE values, mask models were identified as SMs when compliant to DP and BFE performance requirement set by the standard EN 14683:2019, or, differently, as CMs, as shown in Fig. 3.

TABLE I
MAIN SPECIFICATIONS AND CHARACTERISTICS OF THE CMS AND SMS TESTED IN THIS STUDY

Mask ID	Filter material[a]	N° of filter layers	Structure of filter layers[a]	Filter area (cm^2)	Retention system	Nose piece[a]	BFE[b] (%)	DP[c] (Pa/cm^2)
CM01	PP	3	SMS	169	ear loop, elastic	MW	99.6 (0.3)	69 (12)
CM02	92 % cotton, 8 % PU	2	KK	225	ear loop, elastic	none	91.1 (1.3)	56 (3)
CM03	PP	3	SSS	308	ear loop, elastic	none	93.6 (5.6)	10 (0)
CM04	PP	3	SMS	206	ear loop, elastic	MW	95.1 (4.7)	53 (2)
CM05	PP	3	SMS	196	ear loop, elastic	PO	94.7 (4.6)	30 (2)
CM06	PP	1	S	361	ear loop, elastic	none	90.0 (1.5)	11 (1)
CM07	PP	1	S	356	ear loop, elastic	none	90.6 (2.2)	7 (0)
CM08	92 % cotton, 8 % PU	1	K	241	ear loop, elastic	none	91.2 (1.3)	26 (1)
CM09	100 % cotton	2	KK	208	ear loop, elastic	none	87.0 (1.8)	13 (1)
CM10	93 % cotton, 7 % PU	2	KK	218	ear loop, elastic	none	90.5 (1.4)	34 (4)
CM11	PP	3	SMS	228	ear loop, elastic	MW	99.9 (0.1)	88 (12)
CM12	cotton/PP	3	SWS	280	ear loop, elastic	none	82.6 (1.9)	13 (1)
CM13	PP	1	S	323	ear loop, elastic	none	93.2 (2.9)	11 (1)
CM14	cotton/PP	3	SWS	259	ear loop, elastic	MW	85.4 (1.9)	19 (2)
CM15	cotton/PP	4	SWSS	280	ear loop, elastic	none	92.3 (1.4)	23 (2)
CM16	PP	3	SMS	167	ear loop, elastic	MW	100 (0.1)	63 (20)
CM17	PP	3	SMS	174	ear loop, elastic	MW	100 (0.1)	60 (15)
CM18	PP	3	SSS	201	ear loop, elastic	MW	100 (0.1)	92 (4)
CM19	PP	3	SSS	197	ear loop, elastic	MW	100 (0.1)	71 (3)
CM20	PP	3	SSS	207	ear loop, elastic	MW	100 (0.1)	78 (3)
CM21	100 % polyester	1	W	257	ear loop, adjustable length	none	66.3 (8.4)	41 (2)
SM01	PP	3	SMS	198	ear loop, elastic	MW	99.3 (0.1)	42 (4)
SM02	PP	5	SSMSS	225	ear loop, elastic	MW	99.5 (0.4)	46 (5)
SM03	PP	3	SMS	195	ear loop, elastic	PO	96.8 (0.3)	20 (0)
SM04	PP	3	SMS	182	ear loop, elastic	PO	99.7 (0.3)	30 (2)
SM05	PP	3	NMS	229	ear loop, elastic	MW	99.7 (0.2)	27 (15)
SM06	PP	3	SMS	178	ear loop, elastic	MW	99.8 (0.3)	42 (6)
SM07	PP	3	SMS	170	ear loop, elastic	PO	99.8 (0.1)	39 (2)
SM08	PP	3	SMS	178	ear loop, elastic	MW	95.7 (0.8)	32 (3)
SM09	100 % cotton	1	W	296	ear loop, elastic	MW	98.1 (0.5)	53 (0)
SM10	PP	3	SMS	195	ear loop, elastic	MW	99.7 (0.3)	36 (2)
SM11	PP	3	SMS	194	ear loop, elastic	PO	99.9 (0.1)	20 (1)
SM12	PP	3	SMS	178	ear loop, elastic	MW	99.9 (0.1)	40 (8)
SM13	PP	3	SMS	178	ear loop, elastic	MW	100 (0.1)	58 (26)
SM14	PP	3	SMS	188	ear loop, elastic	PO	100 (0.1)	28 (2)
SM15	PP	1	S	361	ear loop, elastic	none	96.0 (3.6)	12 (2)
SM16	PP	3	SMS	187	ear loop, elastic	MW	99.9 (0.1)	48 (9)
SM17	PP	3	SMS	176	ear loop, elastic	PO	99.9 (0.2)	36 (5)
SM18	PP	3	SMS	189	ear loop, elastic	PO	99.6 (0.3)	23 (4)
SM19	PP	3	SMS	200	ear loop, elastic	MW	100 (0.1)	35 (3)
SM20	PP	2	SS	211	ear loop, elastic	none	99.9 (0.2)	37 (0)
SM21	PP	3	SMS	200	ear loop, elastic	MW	100 (0.1)	30 (3)
SM22	PP	3	SMS	202	ear loop, elastic	MW	100 (0.1)	45 (3)
SM23	PP	3	SMS	158	ear loop, elastic	MW	100 (0.1)	40 (5)
SM24	cotton/PP	4	SMSW	217	ear loop, elastic	none	99.9 (0.2)	44 (1)
SM25	PP	3	SMS	233	head loop	none	99.9 (0.2)	35 (2)
SM26	PP	3	SMS	220	ear loop, not elastic	MW	100 (0.1)	33 (1)
SM27	PP	3	SMS	219	ear loop, not elastic	MW	99.9 (0.2)	36 (4)
SM28	PP	3	SMS	248	head loop	none	99.7 (0.3)	38 (6)
SM29	PP	3	SMS	231	ear loop, elastic	MW	99.8 (0.3)	42 (2)

[a.] Abbreviations; PU: polyurethane; PP: polypropylene; S: spunbonded; M: meltblown, N: polypropylene net, MW: metal wire, PO: polymeric band.

[b.] : BFE: Bacterial filtration efficiency according to Annex B ofEN 14683:2019. Values are expressed as mean (standard deviation) of five replicated measurements.

[c.] DP: Breathability according to Annex A of EN 14683:2019. Values are expressed as mean (standard deviation) of five replicated measurements.

With the aim to understand the impact of the sole nosepiece on TFE, a subgroup of 26 masks, randomly selected among those having a nosepiece, was retested according to the experimental protocol reported above, after removing the metallic or polymeric strip at the nosepiece. The strip was carefully removed by sliding it laterally after having performed a small incision on the external filter layer, without altering other mask design characteristics.

F. Measurement Uncertainty

Measurement uncertainty was addressed according to the guidelines in Joint Committee for Guides in Metrology

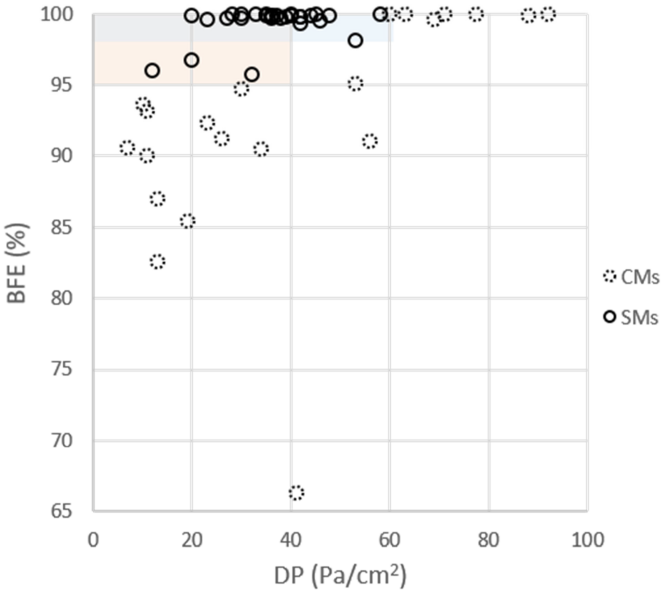

Fig. 3. BFE and DP of the tested masks according to standard EN 14683:2019. Masks models are subgrouped into SMs (solid line circles) when compliant to standard requirement (colored areas: pink for type I and blue for type II-R) and CMs (dashed line circles) when out of standard requirement. Reported values are the mean of five replicated measurements. Dispersions (standard deviations) are listed in Table I.

(JCGM) 100:2008 [50], distinguishing between Type A uncertainty, evaluated by the statistical analysis of series of repeated observations, and Type B uncertainty, evaluated by instrumental accuracy and resolution. The estimator of Type A standard uncertainty for the measurement of any quantity q, directly obtained as the arithmetic mean $\bar{q}$ over N repeated observations q_k, was the standard deviation of the mean $s(\bar{q})$, i.e., the square root of the variance $s^2(q)$ divided by the number of observations

$$u_{\mathrm{A}}(q) = s(\bar{q}) = \sqrt{\frac{s^2(q)}{N}} = \sqrt{\frac{\sum_{k=1}^{N}(\bar{q} - q_k)^2}{N(N-1)}}. \quad (7)$$

Similarly, when the measurement was a predicted value from a linear regression of observations instead of an average, Type A standard uncertainty was obtained by propagating the variances of the slope and the intercept in the interpolant function, dividing by the number of interpolation points, and applying the square root, where slope and intercept variances were calculated by established formulas [50].

Type B standard uncertainty for any measurement derived from DP and airflow rate relied on manufacturer's specifications regarding accuracy of the manometer u_{man} (1% of the read value +1 LSD) and the FM u_{flo} (3% of the read value +1 LSD), respectively. The law of propagation of uncertainty for independent input variables was applied to propagate u_{man} and u_{flo}, and for combining different sources of uncertainty [50].

Experiments of Phase II, measuring $R_{\mathrm{II\ mask}}$ and determining the linear regressor for predicting $R_{\mathrm{I\ mask}}$, were performed once for each mask model. Type A standard uncertainty for the predicted $R_{\mathrm{I\ mask}}$, indicated by $u_{\mathrm{A}}(R_{\mathrm{I\ mask}})$, was computed by propagating slope and intercept variances in the interpolant function. Type B standard uncertainty of $R_{\mathrm{I\ mask}}$, indicated by $u_{\mathrm{B}}(R_{\mathrm{I\ mask}})$, was computed as the average $R_{\mathrm{II\ mask}}$ Type B standard uncertainty $[u_{\mathrm{B}}(R_{\mathrm{II\ mask}})]$ over the 14 measurements, where $u_{\mathrm{B}}(R_{\mathrm{II\ mask}})$ was obtained by propagating u_{man} and u_{flo} in (4)

$$u_{\mathrm{B}}^2(R_{\mathrm{II\ mask}}) = \left(\frac{\Delta P_{\mathrm{II}}}{Q_{\mathrm{II\ mask}}^2}\right)^2 u_{\mathrm{flo}}^2 + \left(\frac{1}{Q_{\mathrm{II\ mask}}}\right)^2 u_{\mathrm{man}}^2. \quad (8)$$

Type A standard uncertainty of BFE, indicated by $u_{\mathrm{A}}(\mathrm{BFE})$, consisted in the standard deviation of the mean over five repeated observations performed according to the method specified in Annex B of standard EN 14683:2019 [16].

The experiments of Phase I for the determination of TFE from ΔP_{I} and $Q_{\mathrm{I\ tot}}$ were performed in quintuplicate by the same researcher for each mask model and flow rate. The mean of TFE over the five replicates ($\overline{\mathrm{TFE}}$) and the standard deviation of the mean $[s(\overline{\mathrm{TFE}})]$, representing the variability from ΔP_{I} and $Q_{\mathrm{I\ tot}}$ observations, were calculated. The overall Type A standard uncertainty of TFE, indicated by $u_{\mathrm{A}}(\mathrm{TFE})$, was then computed combining $s(\overline{\mathrm{TFE}})$ with the Type A contributions from $R_{\mathrm{I\ mask}}$ and BFE propagated in (6)

$$u_{\mathrm{A}}^2(\mathrm{TFE}) = s^2(\overline{\mathrm{TFE}}) + \left(\frac{\Delta P_{\mathrm{I}} \cdot \mathrm{BFE}}{R_{\mathrm{I\ mask}}^2 \cdot Q_{\mathrm{I\ mask}}}\right)^2 u_{\mathrm{A}}^2(R_{\mathrm{I\ mask}}) + \left(\frac{\Delta P_{\mathrm{I}}}{R_{\mathrm{I\ mask}} \cdot Q_{\mathrm{I\ mask}}}\right)^2 u_{\mathrm{A}}^2(\mathrm{BFE}). \quad (9)$$

The overall Type B standard uncertainty for TFE, indicated by $u_{\mathrm{B}}(\mathrm{TFE})$, was computed propagating the instrumental uncertainties (u_{flo} and u_{man}) and Type B contribution of $R_{\mathrm{I\ mask}}$ in (6) according to the following expression:

$$u_{\mathrm{B}}^2(\mathrm{TFE}) = \left(\frac{\Delta P_{\mathrm{I}} \cdot \mathrm{BFE}}{R_{\mathrm{I\ mask}} Q_{\mathrm{I\ mask}}^2}\right)^2 u_{\mathrm{flo}}^2 + \left(\frac{\mathrm{BFE}}{R_{\mathrm{I\ mask}} \cdot Q_{\mathrm{I\ mask}}}\right)^2 u_{\mathrm{man}}^2 + \left(\frac{\Delta P_{\mathrm{I}} \cdot \mathrm{BFE}}{R_{\mathrm{I\ mask}}^2 \cdot Q_{\mathrm{I\ mask}}}\right)^2 u_{\mathrm{B}}^2(R_{\mathrm{I\ mask}}). \quad (10)$$

Finally, the total standard uncertainty for TFE was computed according to

$$u_{\mathrm{tot}}^2(\mathrm{TFE}) = u_{\mathrm{A}}^2(\mathrm{TFE}) + u_{\mathrm{B}}^2(\mathrm{TFE}). \quad (11)$$

G. Statistical Analysis

TFE values were expressed as mean over five replicated experiments and the associated $u_{\mathrm{tot}}(\mathrm{TFE})$. Values of $u_{\mathrm{A}}(\mathrm{TFE})$ and $u_{\mathrm{B}}(\mathrm{TFE})$ were also considered in the interpretation of results.

The results for continuous variables that did not have a normal distribution were presented as median and interquartile interval.

Spearman correlation coefficients were calculated to assess whether a relationship was present between TFE and DP values and between TFE and the mask filter area at flow rates of 30, 90, and 160 L/min.

To investigate the impact of the different design parameters considered in this study, the nonparametric Mann–Whitney U test was used to compare pairs of mask subgroups having different design properties defined by dichotomic variables

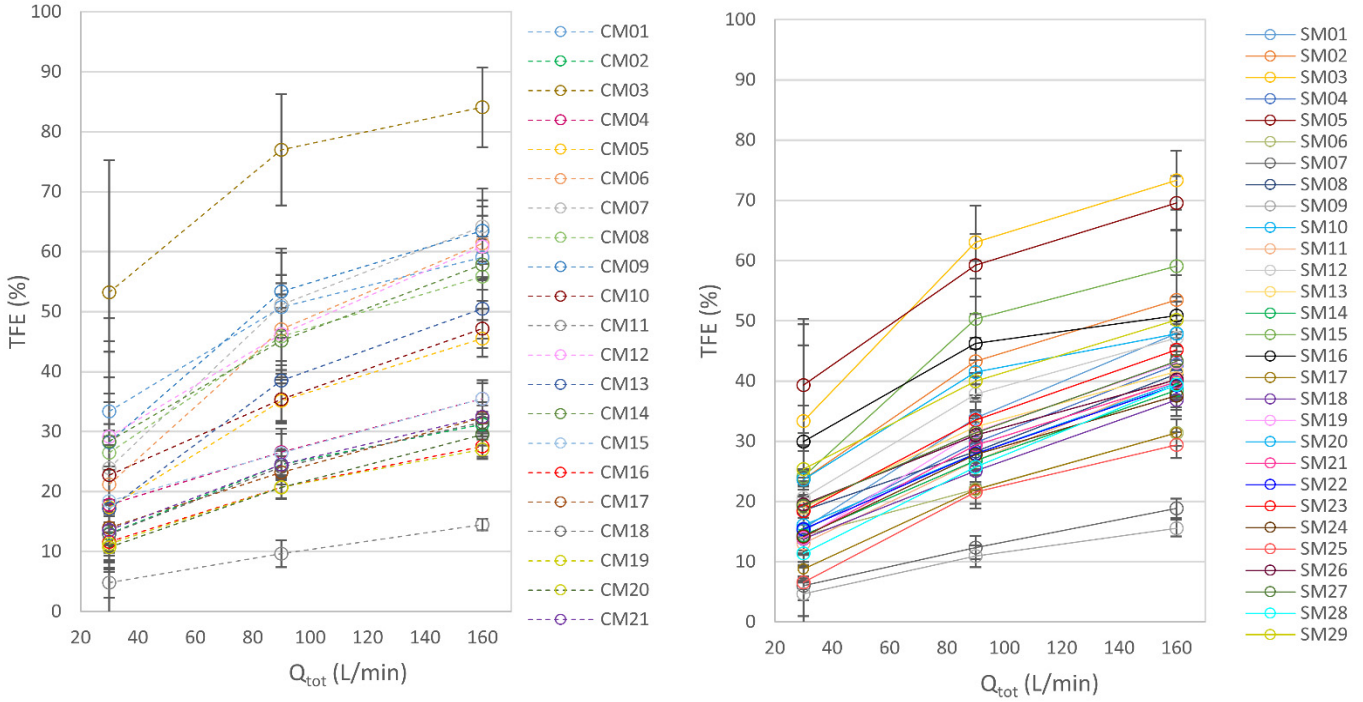

Fig. 4. Percentage of TFE of the tested CMs (dashed line) (left) and the SMs (solid line) (right) in relation to the exhaled airflow rate (Q_{tot}) at 30, 90, and 160 L/min.

(presence/absence of the nosepiece, metallic/polymeric nosepiece, and presence/absence of the meltblown filter layer).

Wilcoxon nonparametric test was used to compare distributions with paired data obtained from testing the subgroup of masks with and without the nosepiece.

All analyses used two-sided tests with a significance level of $p < 0.05$. Statistical analyses were performed using Prism 5 statistical software (GraphPad Software, San Diego, CA, USA).

H. TFE Predictor Model

A response surface method (RSM) [51] was used to model the TFE experimental data. RSM is a collection of mathematical and statistical techniques used in the development of an adequate functional relationship between a response of interest and a number of associated control (or input) variables, called "factors." Using RSM, it is possible to develop empirical polynomial equations relating the response to the factors. This methodology was originally developed to model experimental response [51] and then migrated into the modeling of numerical simulations [52] and observational data [53]. The use of RSM to model observational data was recently summarized in [53]. In our specific case, the factors and their levels were production parameters set by the face mask manufacturers, while the TFE was an experimentally measured output, summarizing mask performance in terms of outward filtration efficacy.

Being TFE expressed as a number ranging 0–1, the following transformation was applied to obtain a normal data distribution:

$$\mathrm{TFE_T} = \arcsin[\sqrt{\mathrm{TFE}}]. \tag{12}$$

The RSM analysis was performed with the programming language R [54] following the statistical strategy and methodological approach described in previous works [55], [56], [57]. Three continuous numerical factors [A-filtering area (cm^2), D-DP (Pa/cm^2), and E-flow rate (L/min)], one discrete numerical factor (B-number of layers), and two categorical factors (F-meltblown and G-nosepiece) were considered.

Since TFE was analytically derived from F_{mask} and BFE, according to (6), we did not consider these two parameters as factors in the model.

The analysis of variance (ANOVA) was used to select the significant terms (having $p < 0.05$) to include in the quadratic model equation having the following general form:

$$\mathrm{TFE_T} = c_0 + \sum_i c_i x_i + \sum_j c_j x_j^2 + \sum_l \sum_l c_{lm} x_l x_m. \tag{13}$$

A quadratic equation was chosen after checking that higher order terms resulted to be aliased and that R^2, the adjusted R^2 (R_A^2), and the predicted R^2 (R_P^2) were maximized, ensuring the minimization of the predicted residual error sum of squares (PRESS). R_A^2 represented the R^2 index adjusted to the numbers of terms inserted in the model (allowing a direct comparison between models with different number of terms), while the R_P^2 indicated how well the regression model predicted responses for new observations. R_P^2 was calculated by excluding one data point from the database, extrapolating the model with the new reduced dataset, and evaluating the ability of the reduced model to predict the excluded datapoint. The process was iteratively repeated for all the datapoints. Similarly, the PRESS was calculated by removing one observation from the dataset and refitting the remaining observations. The out-of-sample predicted value was calculated for the omitted observation in

each case, and the PRESS statistic was calculated as the sum of the squares of all the resulting prediction errors.

The following physical boundary conditions were added outside the range of analysis to guide the empirical prediction of the quadratic model:

$$\text{TFE} = 0 \text{ if } A = 0. \tag{14}$$

According to (14), a set of points with fixed coordinates [Area, DP] = 0, 0 and [Area, DP] = 0, 100 for all the combinations of the categorical and discrete conditions were added to the dataset.

III. Results

A. Total Filtration Efficiency

TFE values obtained at low (30 L/min), medium (90 L/min), and high (160 L/min) outward flowrates are summarized in Table II and graphically depicted in Fig. 4 for each of the 50 tested masks. TFE associated uncertainties (u_{tot}), including Type A (u_A) and Type B components (u_B), are also indicated in Table II.

For sake of clarity, results were grouped by CMs and SMs. Remarkably, TFE values ranged over a large interval (from 5% to 73%) depending on the single mask model and the outward flow rate.

For all tested masks, TFE values systematically increased with the outward flow rates. The median [first quartile; third quartile] values of TFE over the whole tested masks were 17[14; 24]% at 30 L/min, 30[25; 43]% at 90 L/min, and 41[33; 51]% at 160 L/min. No significant differences were found between CMs and SMs subgroups in terms of TFE at the three tested flow rates.

The uncertainty u_{tot}(TFE) associated with each TFE measurement is reported in Table II, including its instrumental and repeatability components. The total TFE uncertainty ranged among all tested masks varied from 2% to 25% at 30 L/min, from 2% to 10% at 90 L/min, and from 1% to 8% at 160 L/min. In general, u_{tot}(TFE) of all tested masks decreased with the increasing of the flow rate applied during the test, with a median [first quartile; third quartile] value of 6[5,8]%, 3[3,5]%, and 3[3,4]%, respectively, at 30, 90, and 160 L/min. When testing low DP masks at low flow rates, u_{tot}(TFE) was generally dominated by the instrumental uncertainty, u_B(TFE).

In these conditions, the instrumental accuracy of the DP measurement system was comparable to the DP itself. Differently, experimental repeatability impacted less on u_{tot}(TFE), with u_A(TFE) ranging from 0% to 3% at 30 L/min, from 0% to 2% at 90 L/min, and from 0% to 3% at 160 L/min.

The correlation analysis between the single design parameters and TFE showed significance only for DP (filter breathability) and the presence of the nosepiece, addressed in detail below, while no correlation with TFE was detected for mask area, the number of layers, and the presence of a meltblown layer.

B. Role of the Mask Filter Breathability

The correlation between TFE values and breathability of the mask filter (DP) is shown in Fig. 5. At all the three tested outward flow rates (30, 90, and 160 L/min), the higher the DP values, the lower the TFE of the mask. Results of the Spearman's test indicated a significant ($p < 0.05$) monotonic negative correlation between TFE and DP. The correlation strength was moderate (Spearman's rho = −0.45 and −0.57 at a flow rate of 30 and 90 L/min, respectively) and strong (Spearman's rho = −0.61 at a flow rate of 160 L/min).

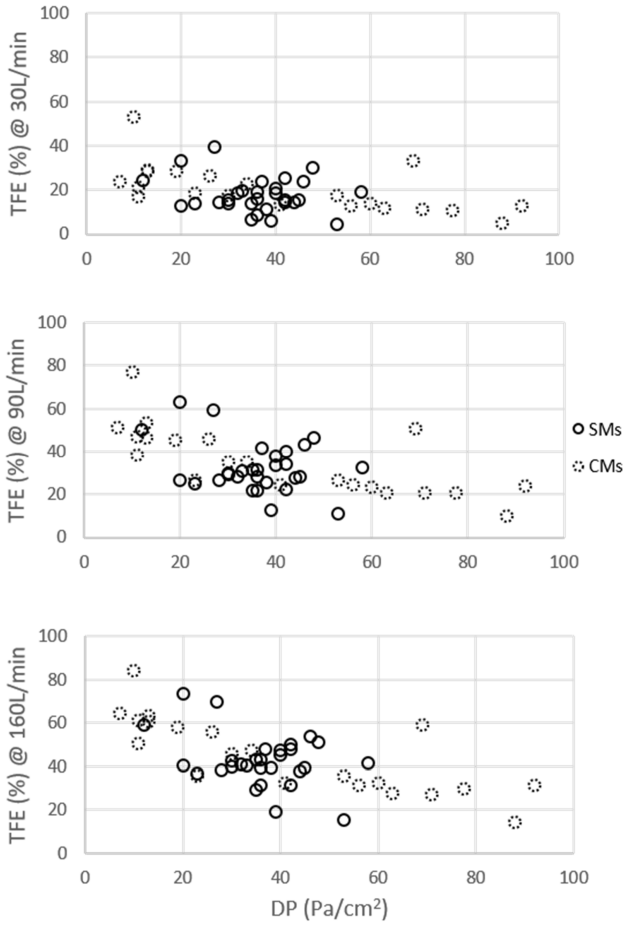

Fig. 5. Scatterplot of the TFE of each mask versus the mask filter breathability (DP). From top to bottom, data are presented for total exhaled airflow rates of 30, 90, and 160 L/min. Dashed circles indicate CMs, while continuous circles indicated SMs.

C. Role of the Nosepiece

Results of the TFE measurements performed on the subset of 26 masks with the original nosepiece installed by the mask manufacturer (w/ NP) and after removal of the nosepiece (w/o NP) are presented as paired measurements in Fig. 6.

Most of 26 tested masks showed lower TFE values without the nosepiece, irrespectively of the outward flow rate. Indeed, the median [first quartile; third quartile] values of TFE measured without nosepiece at the three flow rates were 12[9,15]%, 21[17,29]%, and 32[25,39]%, respectively. With the nosepiece in place, the same group of masks tested in identical testing conditions presented TFE values of 15[13,19]%, 28[22,33]%, and 40[31,45]%. The comparison of TFE values obtained with and without nosepiece over the 26 tested masks indicated that a significant increase in TFE was achieved when the nosepiece was present ($p < 0.05$, Wilcoxon rank-sum test).

TABLE II

TFE OF THE TESTED COMMUNITY AND SMS, AND TOTAL UNCERTAINTY (u_{tot}) CALCULATED ACCORDING TO (10), WITH ITS COMPONENTS (u_A, u_B) IN DETAIL. DATA ARE REPORTED FOR LOW (30 L/MIN), MEDIUM (90 L/MIN), AND HIGH (160 L/MIN) FLOW RATES

ID mask	TFE (%)											
	@ 30 L/min				@ 90 L/min				@ 160 L/min			
	Mean	u_{tot}	u_A	u_B	Mean	u_{tot}	u_A	u_B	Mean	u_{tot}	u_A	u_B
CM01	33.4	5.1	0.8	5.0	50.7	3.9	0.8	3.9	59.1	3.8	0.4	3.8
CM02	13.0	3.5	0.2	3.5	24.5	2.1	0.4	2.1	31.2	2.2	0.3	2.1
CM03	53.2	19.7	1.8	19.6	77.0	10.0	2.5	9.7	84.1	8.3	2.5	7.9
CM04	17.8	6.3	0.4	6.3	26.6	3.1	0.8	2.9	35.5	3.0	0.9	2.8
CM05	17.3	6.2	0.5	6.1	35.1	3.5	1.0	3.4	45.5	3.5	1.1	3.3
CM06	21.2	21.6	0.6	21.6	47.1	9.4	1.4	9.3	61.4	7.7	1.1	7.6
CM07	23.9	24.9	0.8	24.9	51.1	10.3	1.2	10.3	64.2	8.2	1.1	8.2
CM08	26.5	9.4	0.4	9.4	45.9	4.9	0.5	4.9	55.8	4.6	0.5	4.6
CM09	28.3	13.6	2.6	13.4	53.4	6.8	0.6	6.7	63.5	6.1	0.8	6.1
CM10	22.8	6.2	0.3	6.2	35.4	3.5	0.6	3.4	47.2	3.5	0.5	3.5
CM11	4.8	2.5	0.1	2.5	9.7	2.3	0.1	2.3	14.5	1.1	0.1	1.1
CM12	29.2	15.3	0.5	15.3	46.3	6.9	0.6	6.9	60.9	6.3	0.9	6.2
CM13	17.2	17.5	0.5	17.4	38.5	7.4	1.3	7.2	50.5	5.8	1.2	5.7
CM14	28.4	10.2	0.5	10.1	45.2	5.1	0.6	5.1	57.8	4.9	0.7	4.8
CM15	18.4	10.8	2.0	10.6	26.4	4.2	0.3	4.2	35.5	3.5	0.5	3.5
CM16	11.6	3.2	0.1	3.2	20.7	1.9	0.4	1.9	27.5	1.9	0.2	1.9
CM17	14.0	3.8	0.1	3.8	23.2	2.1	0.2	2.1	32.3	2.2	0.2	2.2
CM18	12.9	2.7	0.6	2.7	24.1	1.9	0.3	1.8	31.5	2.1	0.3	2.0
CM19	11.3	3.1	0.1	3.1	20.7	1.8	0.3	1.8	27.1	1.8	0.2	1.8
CM20	10.7	3.3	0.7	3.2	20.7	1.8	0.3	1.8	29.5	2.0	0.4	2.0
CM21	13.6	4.6	1.2	4.5	24.5	2.8	1.4	2.4	32.5	3.1	1.9	2.5
SM01	15.5	5.5	0.3	5.5	33.9	3.1	0.9	3.0	47.9	3.4	0.4	3.4
SM02	23.7	5.1	1.1	4.9	43.3	3.6	0.9	3.4	53.5	3.8	1.1	3.6
SM03	33.4	11.4	2.2	11.2	63.1	6.5	1.2	6.4	73.3	5.8	1.2	5.7
SM04	15.2	7.9	0.2	7.9	29.8	3.6	0.4	3.6	42.7	3.5	0.4	3.5
SM05	39.3	9.7	2.1	9.5	59.3	5.6	0.4	5.6	69.6	5.2	0.3	5.2
SM06	14.4	5.1	0.3	5.1	22.0	2.4	0.5	2.4	31.4	2.4	0.5	2.3
SM07	6.0	4.6	1.1	4.5	12.4	1.8	0.4	1.8	18.9	1.6	0.3	1.6
SM08	18.5	6.6	0.4	6.6	28.3	3.2	0.6	3.1	41.2	3.2	0.4	3.2
SM09	4.7	4.8	0.1	4.8	10.9	1.8	0.1	1.8	15.6	1.4	0.3	1.4
SM10	16.1	6.2	1.2	6.1	27.9	2.9	0.5	2.8	39.6	3.0	0.4	3.0
SM11	13.1	8.5	2.0	8.3	26.7	3.6	0.3	3.6	40.5	3.4	0.3	3.4
SM12	20.6	4.1	0.7	4.0	37.8	2.9	0.3	2.9	47.1	3.1	0.3	3.1
SM13	19.0	4.3	0.2	4.3	32.4	2.7	0.5	2.7	41.6	2.8	0.3	2.8
SM14	14.4	7.5	0.2	7.5	26.8	5.0	0.6	5.0	38.5	3.2	0.4	3.2
SM15	24.2	24.6	0.6	24.6	50.3	9.9	1.7	9.7	59.1	7.8	1.1	7.8
SM16	29.9	5.3	0.9	5.3	46.2	4.1	1.5	3.8	50.9	3.4	0.4	3.4
SM17	8.8	6.6	0.1	6.6	22.0	3.9	0.2	3.9	31.4	4.6	0.3	4.6
SM18	13.8	7.1	0.2	7.1	25.1	3.1	0.3	3.1	36.9	3.1	0.4	3.1
SM19	13.9	5.7	1.3	5.5	31.6	3.0	0.8	2.9	43.1	3.1	0.4	3.1
SM20	23.6	5.3	0.3	5.3	41.5	3.7	0.9	3.5	47.9	3.3	0.4	3.3
SM21	14.1	5.5	0.2	5.5	29.3	5.2	0.6	5.2	39.9	6.6	0.5	6.6
SM22	15.4	4.9	1.1	4.8	28.0	2.7	0.5	2.6	39.3	2.8	0.3	2.8
SM23	18.4	6.4	1.2	6.3	33.5	3.4	0.8	3.4	45.2	3.3	0.3	3.3
SM24	14.2	4.6	1.0	4.4	27.8	2.5	0.4	2.5	37.6	2.6	0.3	2.6
SM25	6.6	6.7	0.1	6.7	21.6	2.9	0.4	2.8	29.4	2.5	0.4	2.5
SM26	19.5	5.3	0.2	5.3	31.0	2.9	0.4	2.8	40.3	2.9	0.3	2.9
SM27	19.3	5.3	0.2	5.3	31.4	2.8	0.4	2.8	43.3	3.1	0.2	3.1
SM28	11.4	5.9	0.1	5.9	25.7	2.9	0.5	2.8	39.4	3.0	0.3	3.0
SM29	25.4	5.8	0.3	5.7	40.0	3.5	0.5	3.5	50.2	3.5	0.3	3.5

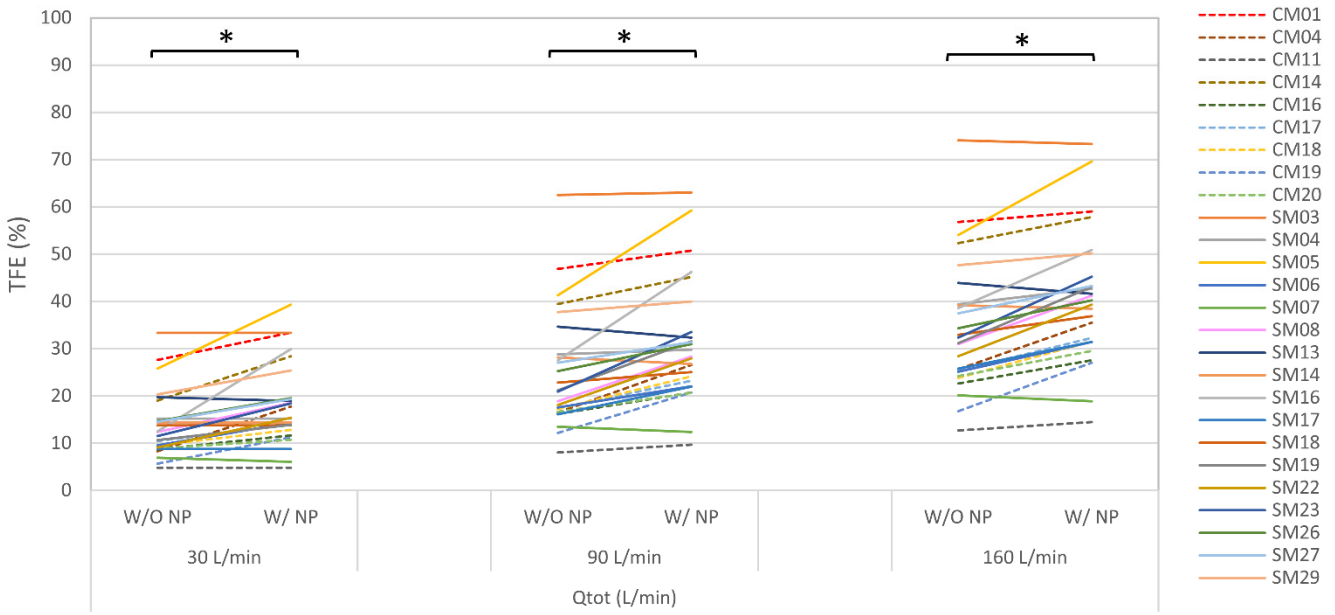

Fig. 6. TFE of face masks ($N = 26$) with (w/ NP) and without (w/o NP) nosepiece. Data are presented for three different flow rates of 30, 90, and 160 L/min. Each colored line (dashed for CMs and continuous for SMs) indicates the performance of the same mask with and without the nosepiece. $^{*}p < 0.05$.

However, six masks out of 26 showed no changes in TFE with or without the nosepiece when tested at 30 L/min, and 2, 3, and 4 masks out of 26 showed an increase of TFE when tested without nosepiece at 30, 90, and 160 L/min, respectively. Usually, the increase or decrease in TFE was consistent for the same mask across the three tested flow rates conditions.

To better quantify the variation of TFE with respect to the presence/absence of the nosepiece, the difference between the TFE values obtained from the same mask with and without nosepiece was calculated and identified as ΔTFE. The median values [first quartile; third quartile] of ΔTFE over the 26 tested masks were 4[0,6]%, 5[2,9]%, and 6[3,10]% at a flow rate of 30, 90, and 160 L/min, respectively, being influenced by the general increase of TFE with the increase of the outward airflow.

The ΔTFE was then analyzed distinguishing between nosepieces made of or incorporating a metal wire (MW) and those made only by a polymeric band (PO). Fig. 7 shows that ΔTFE obtained when MW nosepieces are applied is significantly higher than those obtained by applying a PO nosepiece. Differences between MW and PO subgroups were statistically significant at all the three tested flow rates. ($p < 0.05$, Mann–Whitney U test). A median ΔTFE of 5%, 6%, and 7% was associated with the use of an MW nosepiece when the outward airflow was 30, 90, and 160 L/min, respectively, with a maximum value of 19% reached by SM16 at 90 L/min.

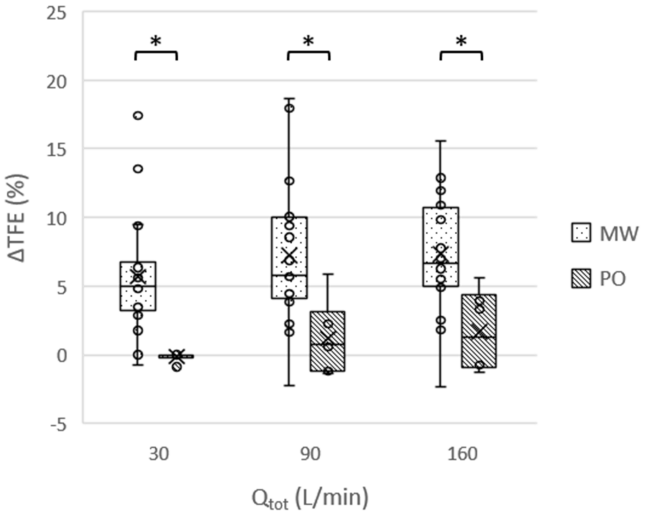

Fig. 7. ΔTFE (%) (i.e., difference of TFE values measured with and without nosepiece) according to the type of nosepiece: MW and PO. Data are presented at three different flow rates. $^{*}p < 0.05$.

D. Response Surface Method

The RSM could identify a model that well-fit the collected data ($R^2 = 0.87$), as shown in the actual versus predicted Fig. 8 (left). Despite small deviation from normality in the residuals distribution, as shown in Fig. 8 (right), residuals were acceptable to perform reliable predictions.

ANOVA results (Table A of the supplementary material) showed that the quadratic model was statistically significant (F-value = 110.88, p-value < 0.0001) with only a 0.01% chance that an F-value this large could have occurred due to noise. The model terms A, B, D, E, G, AD, AE, BF, BG, DF, DG, A^2, B^2, and E^2 were statistically significant, with a p-value lower than 0.05. Although not significant, the term F was included to maintain the model hierarchy, due to the presence of high-order significant terms (BF and DF). The quadratic model was the higher order model to avoid aliasing among the different terms (Table B of supplementary material) and to maximize R^2_A and R^2_P (Table C of the supplementary material). The good agreement of R^2_A and R^2_P with the calculated R^2 ensured a model without over or under fitting and with a good predictivity (Table D of supplementary material).

Estimates of the coefficients of the linear quadratic model are reported in Table III with their associated standard errors

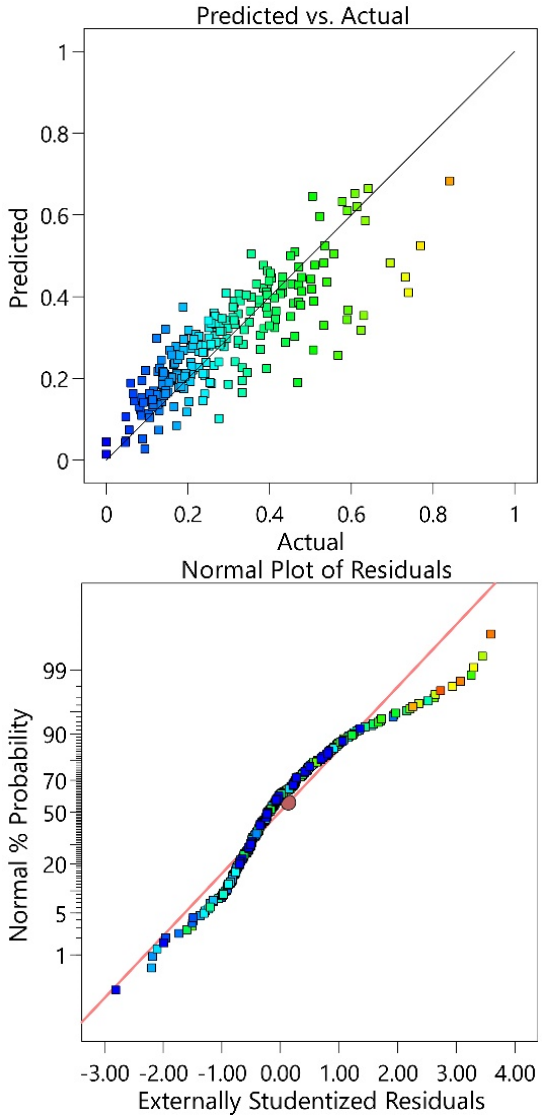

Fig. 8. Actual (experimentally collected) versus predicted (according to the model identified with the RSM) TFE values (top image). Normalized plot of residuals, showing some deviations from residual normality (bottom image), but acceptable for the validity of the model.

and 95% confidence intervals (CIs). Estimated coefficients were calculated based on the normalized model, in which each factor was normalized in the [−1, 1] range. This allows a direct evaluation of the factor's impact on TFE.

TFE results computed according to the quadratic RSM model were plotted on bidimensional surface plots, indicating TFE as a function of mask area and filter DP. Surface plots were presented for different scenarios, according to the values assumed by the categorical variables. Only the surfaces where datapoints were present are shown in Figs. 9–12.

The negative linear coefficient of DP (factor D) dominates the RSM model, causing TFE to decrease within the range of 7–92 Pa/cm^2 at higher DP values in all scenarios, consistently with the trend of the data presented in Fig. 5. TFE is also significantly affected by the flow rate in all scenarios, showing an increase for higher flow rates in accordance with the results of Fig. 4. Minor variations in TFE appeared according to mask areas in the range 158–361 cm^2, with a maximum reached

TABLE III

ESTIMATION OF THE COEFFICIENTS OF THE NORMALIZED MODEL, ASSOCIATED STANDARD ERROR, AND 95% HIGH AND LOW CIS. FACTORS WERE NORMALIZED BETWEEN −1 AND 1

Factor	Coefficient Estimate	Standard Error	95 % CI Low	95 % CI High
Intercept	0.5561	0.0177	0.5213	0.5909
A-Filtering area	-0.0754	0.0332	-0.1408	-0.0100
B-n Layers	0.0639	0.0287	0.0074	0.1204
D-DP	-0.2393	0.0210	-0.2807	-0.1979
E-Flow Rate	0.1574	0.0100	0.1377	0.1772
F-Melblown	0.0100	0.0094	-0.0085	0.0286
G-Nose piece	-0.0371	0.0072	-0.0512	-0.0229
AD	-0.1257	0.0134	-0.1522	-0.0992
AE	0.0565	0.0086	0.0395	0.0734
BF	-0.0948	0.0357	-0.1650	-0.0245
BG	-0.0563	0.0199	-0.0956	-0.0171
DF	-0.0573	0.0156	-0.0881	-0.0266
DG	-0.0255	0.0121	-0.0494	-0.0017
A^2	-0.1025	0.0126	-0.1272	-0.0777
B^2	-0.1159	0.0344	-0.1837	-0.0482
E^2	-0.0332	0.0129	-0.0586	-0.0078

within the middle range 200–300 cm^2, a trend related to the negative coefficient of factor A^2 in the model.

The highest values in TFE (above 70%), within the explored domain of DP and areas values, appeared in the scenario where a 160-L/min outward flow is exhaled against a three-layer mask equipped with the nosepiece, but no meltblown (Fig. 10). Increasing the number of layers improves TFE only when a nosepiece is in place, both with or without meltblown present (Figs. 10 and 12), indicating that only when the fitting is improved by a nosepiece, a thicker material can improve performance, since the leakage caused by the lower breathability is mitigated by the tighter fitting. In the model, the presence of a meltblown layer is associated with a slightly decrease of the TFE in the lower DP region of the surface plots (Figs. 9 and 10 versus Figs. 11 and 12), but it is worth noting that few datapoints are present there (it is challenging to obtain an effective meltblown with a low DP, and therefore, in our mask sample, there was with these characteristics), attenuating the meaning of this prediction.

Regarding the effect of the nosepiece, the predicted TFE values are higher when a nosepiece is in place, especially when a meltblown layer is present in the mask filter (Fig. 11 versus Fig. 12), and minorly when no meltblown is used (Fig. 9 versus Fig. 10). This trend indicates that when a good filtering material with a higher DP is used, the nosepiece can reduce leakage improving mask performance, but the benefit is marginal for cloth mask with a lower DP.

The standard error and the width of the 95% CI of the model coefficients quantify the impact of each factor in terms of model uncertainty. The first-order terms in decreasing order of contribution were the filtering area, the number of layers, the DP, the flow rate, the meltblown, and the nosepiece. However, the mixed term of the meltblown and the DP and the second-order term related to the number of layers had a higher contribution than the first-order terms.

IV. DISCUSSION

Experimental data showed that TFE increases at higher flow rates, coherently over all the tested masks. This behavior

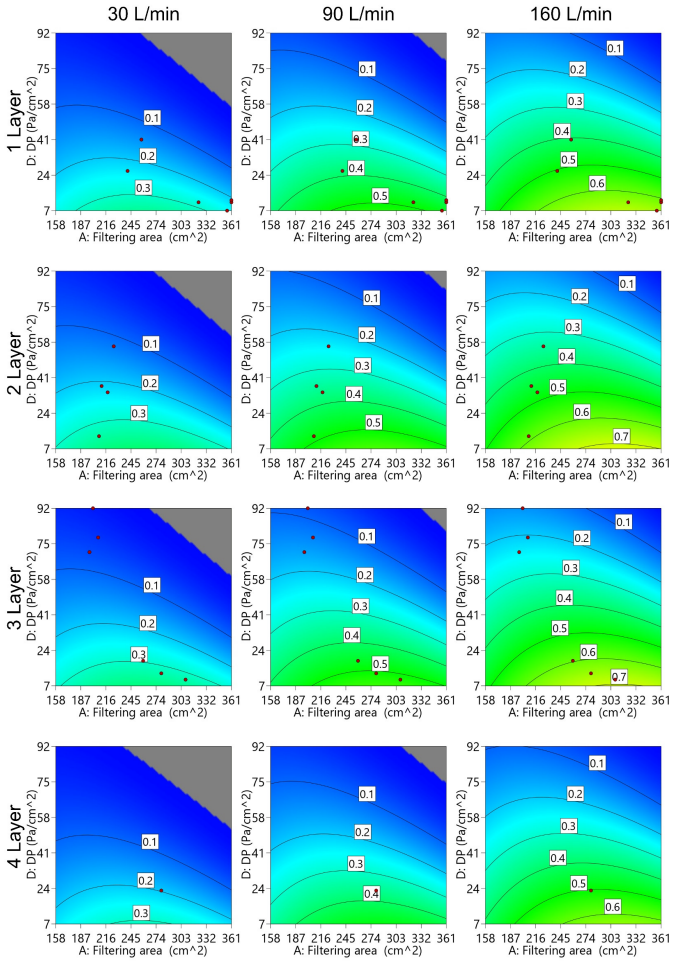

Fig. 9. TFE values predicted by the RSM model for a mask with no meltblown layer in the filter and no nosepiece. Results are shown at three different flow rates (30, 90, and 160 L/min). Experimental datapoints are represented with red dots.

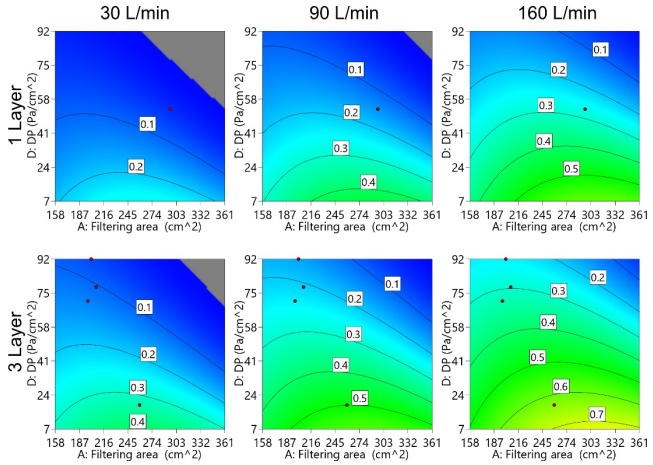

Fig. 10. TFE values predicted by the RSM model for a mask with no meltblown layer in the filter, but a nosepiece in place. Results are shown at three different flow rates (30, 90, and 160 L/min). Experimental datapoints are represented with red dots.

confirmed our previous results on a smaller number of mask models [27], and it is consistent with the opposite behavior observed for the fraction of air leaking at the face seal, that is reduced at higher flow rates [43], [58]. This is a consequence of the complementary role of Q_{mask} and Q_{leak} in (1) and the role of Q_{mask} in the definition of F_{mask} (5) and TFE (6). It is important to emphasize that since TFE is a percentage measure of outflowing filtered air, the increase of TFE at higher flow rate, which could be typical of heavy breathing or loud vocalization, is not enough to cause a decrease of the absolute amount of aerosol emitted by the mask wearer. In fact, such activities have been associated with greater aerosol emission [59].

The analysis of breathability and TFE data showed a negative monotonic correlation at all flow rates, in particular at 160 L/min. The surface response model confirmed this trend, producing a large negative linear coefficient associated with DP. This reinforced the concept that highly breathable materials can improve the mask efficiency, facilitating the passage of the airflow through the mask filter and avoiding leakages, supporting the results previously obtained by Chiera et al. [43]. It is interesting to note that no significant difference in TFE existed between community and SMs, with some CMs (e.g., CM03) showed higher TFE values than many of the SMs tested in this study. This ensues from a less marked contribution of BFE on TFE calculation than F_{mask}. Indeed, although many CMs have moderately lower BFE values than a typical SM, most of them, in our mask sample, were also characterized by far lower DP values. As previously reported [43], breathability has a strong correlation with the fraction of airflow leaking at the face seal since leakage is facilitated when the airflow encounters a high filter resistance [24], [60]. As leakage is complementary to F_{mask}, which is the dominant factor on TFE, a better breathability may significantly enhance TFE.

The effect of DP on TFE has been analyzed in other works, reinforcing the importance of tissue breathability and a proper fit. For instance, Freeman et al. [21] tested aerosol overall FE of masks mounted on a manikin head at constant inflow and outflow rates, in sealed and unsealed configurations. While in sealed conditions fabric weight and thickness correlated positively with FE, the performance for unsealed configurations was remarkably inferior, evidencing the role of leakage in reducing the benefit of the sole material FE of a mask in real world usage. Pan et al. [34] evaluated face covering for material FE and inward/outward protection efficiency at different aerosol sizes, confirming that material FE can misrepresent the protection efficiency of a worn mask due to fitting. Protection efficiency varied also with aerosol size, being above 50% and 75% for particles larger than 1 μm for a homemade CM and an SM, respectively, but decreasing consistently for smaller aerosols. Lindsley et al. [35] studied how performance metrics such as FE, fit factor, and airflow resistance can represent the actual efficiency of a mask, measured as collection efficiency of artificial aerosol emitted from a manikin head form with pliable skin. Collection efficiency of exhaled aerosols ranged 42%–99% for medical masks and 17%–66% for CMs. Correlation of collection efficiency with FE, fit factor, and airflow resistance was significant but not strong enough to make these alternative performance metrics good predictors for the actual performance, with variability in seal leakage and particle size considered as the interfering

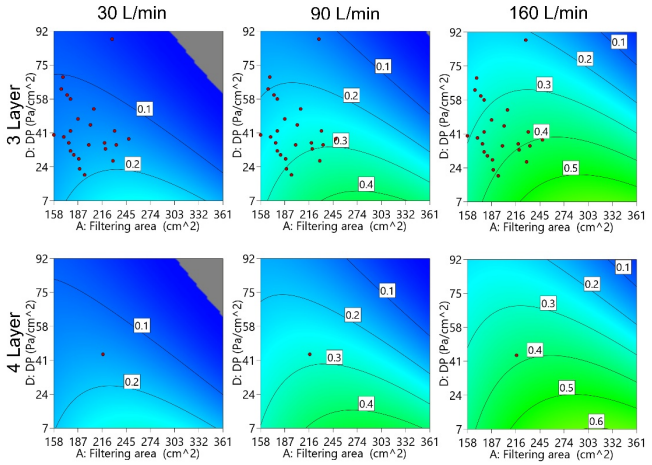

Fig. 11. TFE values predicted by the RSM model for a mask with a meltblown layer in the filter, but no nosepiece. Results are shown at three different flow rates (30, 90, and 160 L/min). Experimental datapoints are represented with red dots.

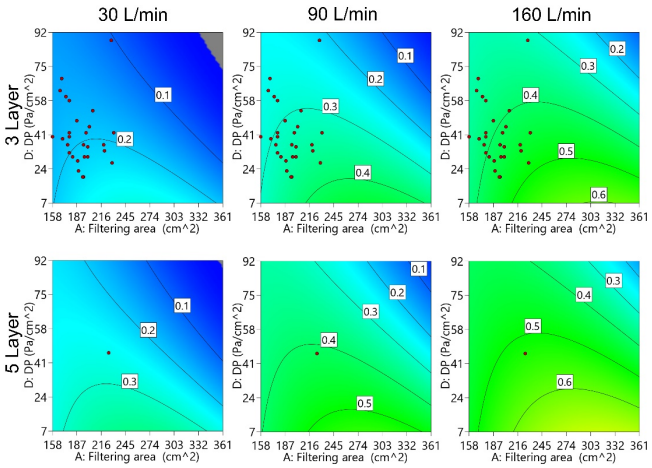

Fig. 12. TFE values predicted by the RSM model for a mask with a meltblown layer in the filter and a nosepiece in place. Results are shown at three different flow rates (30, 90, and 160 L/min). Experimental datapoints are represented with red dots.

factors for the correlation. These observations are compatible with our results regarding the trend and the spread of TFE data with respect to material breathability and BFE although a straight comparison between collection efficiency and TFE is improper. Since the former is a direct measure of aerosol filtration, the latter is an estimate from mask leakage and BFE, where the effects of inertial impaction and different aerosol size are not considered.

Computational fluid dynamics (CFD) simulations [38], [61] have been conducted to study the airflow pattern around a worn mask during breathing and coughing, evidencing how misfitting a mask create leakage through gaps compromising its efficacy [61], and that leakage correlates with lower filter porosity because of the increased DP of the filtering materials [38]. All these results corroborate the recommendation for a tight fitting and a breathable material, and the necessity of identifying comprehensive performance metrics which include the effect of leakage, such as the TFE defined in this study.

To further investigate the role of the seal, we tested the subgroup of 26 masks marketed with a nosepiece also after removing the nosepiece. We found that the presence of the nosepiece positively correlated with TFE at all three flow rates. The type of the nosepiece also affected the results, with an MW strip associated with a much better efficiency at reducing the leakage than a PO. This finding may be ascribed to the better pliability of metal when adapting the nosepiece to the user's nose ridge and its capability to maintain the shape. The surface response model confirmed the importance of the nosepiece in improving TFE performance, differentiating according to the presence of a meltblown layer, where the effect was more pronounced. These results underline the importance of the nosepiece in mask design, especially with filtering materials which offer a lower breathability, and are consistent with studies performed on human subjects [20] and with computational simulations [38], showing that air escaping from the gaps around the nose is more critical than lateral leakage.

The role of other parameters involved in mask design (mask area, the number of layers, and the presence of the meltblown) on the TFE was also investigated. While the analysis of the single factors did not detect any significant correlation with TFE apart from DP, the surface response model evidenced an influence of several factors on TFE. There was a minor negative quadratic variation of TFE with the mask area, with a maximum in the middle range. This trend could be ascribed to the fact that only the mask surface region around the mouth was involved in air filtering, while exceeding tissue wrapped toward the ears and under the chin offered a poor contribution. Concerning the design of tissue material, i.e., the number of layers and meltblown, while they improve material FE, they also worsen filter breathability, canceling out any benefit for masks with a poor seal. However, the surface response model showed that increasing the number of layers (up to 3) can enhance performance when a nosepiece is present, i.e., when the seal of the mask is good enough to contain the leakage due to an increase in DP.

The uncertainty associated with experimental TFE measurements might suggest a more extensive use of CFD simulations. Despite the interesting possibility to visualize the behavior of flow and particles through mask and face-seal leaks, its exploitation has been hindered by several factors. The typical approach is based on fixed geometries of the masks, thus neglecting the fluid-structure interaction between flow and mask (which is instead inherently reproduced in the laboratory test). It is well-known that inward and outward flows have very different effects on the protection offered by the mask [24]. On the one hand, inhalation generates a low pressure on the inner side of the mask, thus sealing or at least reducing perimeter leaks. On the other hand, exhalation increases the internal pressure, inflating the mask and increasing the perimeter leakages. This phenomenon is further amplified in the case of coughing and sneezing.

Another aspect worth to be mentioned is the impact of leak area on the amount of leaked flow and ultimately on the FE. CFD studies showed that gap heights greater than 0.2 mm can generate a total inward leakage larger than 2%, thus making ineffective even an filtering face piece 3 (FFP3) mask, while, for a 1 mm height, more than 70% of flow can be leaked unfiltered [58]. Xi et al. [61] performed CFD simulations

with an SM geometry reconstructed by images of an SM and studied the impact of variable face-seal gaps on the amount of leaked flow. Interestingly, they observed that even a small gap of 0.5 cm^2 leads to a 9% leakage. Considering that 3-D optical scanners have hardly a resolution <0.1 mm (unless choosing very expensive products and small measurement volume), this makes the comparison between numerical studies and experimental tests very challenging. In fact, even a small error on the 3-D reconstruction of the face-mask assembly can return a significant misprediction of the leaked flow. This is also confirmed by the very limited validations of the CFD results, considering, at best, a benchmark in terms of velocity at a point and associated with large error bars [61].

Despite these limitations, numerical investigations by Solano et al. [38], Solano and Shoele [62], and Xi et al. [61] confirmed that a high-porosity mask (i.e., with higher breathability) reduces the edge leakages, especially in the presence of small gaps. These findings not only confirm the validity of the conclusions highlighted in this work, but suggest that an optimum tradeoff can be identified in terms of porosity and safety.

Overall, these considerations make more convenient and reliable to perform this kind of investigations with the two-phase method developed in [23] and applied in this work.

A. Study Limitations

The experimental method to determine TFE of face masks was based on the measurement of the fraction of exhaled air leaking at the face seal and the fraction of exhaled air passing through the mask filter. Two assumptions were made. First, the volume of air passing through the filtering material of a mask is subjected to FE equal to the BFE measured according to the EN 14683:2019 standard. Second, the fraction of air leaking at the face seal moves from the mouth to the external environment without undergoing any change in the amount and size distribution of the aerosol generated by the mask wearer. Under these circumstances, the measured TFE does not consider impaction filtration mechanisms that could be active in reducing droplet amount both for the fraction of air passing through the mask filter and that passing at the face seal. Therefore, TFE values determined according to the presented method represent a worst-case scenario; defining the lower value of filtration performance, a mask can show when only fine aerosol (<5 μm) is exhaled by the wearer. The existence of different processes for blocking particles than through-mask filtration has been observed by Lindsley et al. [35], ensuing from a collection efficiency in the same cases larger than the material FE. Cappa et al. [20] conducted an in-depth analysis of aerosol concentration in mask leakage exhaled during talking and coughing in human subjects. While air leakage reduced mask performance (from >90% to 70% for talking), particle concentration in leaked air was lower than in the original source, implying the effect of an impact mechanism on the inner surface of the mask, especially for larger particles [20]. This observation suggests that SMs can significantly reduce emission of large particles even in the presence of unfiltered leaked air. Even though the TFE may not represent an absolute measurement of mask performance in relation to COVID-19 transmission because of this bias, it is still informative to assess the relative performance among different masks and to detect correlations with constructive and fitting parameters that may guide mask design to improve its efficacy.

A second limitation of the proposed measuring methods is related to the nonnegligible uncertainty associated with the TFE measurement. Although the repeated experiments resulted in a good measurement repeatability in most of the cases, u_B(TFE) was markedly higher than u_A(TFE), due to the propagated uncertainty generated by the accuracy of the FM and the manometer we used. Type B uncertainty may include residual systematic biases which are not corrected by the manufacturer calibration and not accounted in Type A uncertainty, which was obtained by repeated observations performed with the same instrument. This aspect can be improved by using instrumentation with higher accuracy across the whole range of interest of DP and volumetric airflow.

Other than this, variability among masks from the same production batch was previously evidenced in [42] and [63], possibly impacting on ΔP measurement repeatability more than other sources of uncertainty.

Other limitations of the setup were previously identified [27] and were mainly related to the smooth and rigid surface of the head form, different from the skin. Elasticity and compliance of human skin can result in a better face fit and face seal [64]. In this case, our experimental conditions may cause the TFE to be underestimated. Nevertheless, the proposed methodology remains safely applicable for comparative TFE measurements between different masks.

V. Conclusion

The performance of SM and CM in terms of TFE is strongly affected by the mask filter breathability, recommending the selection of highly breathable materials in mask design to decrease air leaking, besides maximizing user comfort and compliance in wearing the face mask. When multiple filter layers are required and a lower breathability is obtained, TFE should be improved by focusing on mask fit and applying a metallic nosepiece. The same recommendation applies when a meltblown layer is present, given the nonnegligible impact of this layer on the filter breathability. On the other hand, providing that only layers with high breathability are used, CMs may offer an acceptable efficacy, in the context of their intended use, without requiring the inclusion of a nosepiece in their design.

Acknowledgment

The authors warmly thank Dr. Manuel Tomasi for printing the 3-D head form.

References

[1] A. A. Aliabadi, S. N. Rogak, S. I. Green, and K. H. Bartlett, "CFD simulation of human coughs and sneezes: A study in droplet dispersion, heat, and mass transfer," in *Proc. ASME Int. Mech. Eng. Congr. Expo.*, Jan. 2010, pp. 1051–1060, doi: 10.1115/IMECE2010-37331.

[2] N. Leung et al., "Respiratory virus shedding in exhaled breath and efficacy of face masks," *Nature Med.*, vol. 26, pp. 676–680, May 2020, doi: 10.1038/s41591-020-0843-2.

[3] J. Cai, W. Sun, J. Huang, M. Gamber, J. Wu, and G. He, "Indirect virus transmission in cluster of COVID-19 cases, Wenzhou, China, 2020," *Emerg. Infectious Diseases*, vol. 26, no. 6, pp. 1343–1345, Jun. 2020, doi: 10.3201/eid2606.200412.

[4] C. Xie et al., "The evidence of indirect transmission of SARS-CoV-2 reported in Guangzhou, China," *BMC Public Health*, vol. 20, no. 1, p. 1202, Aug. 2020, doi: 10.1186/s12889-020-09296-y.

[5] C. R. MacIntyre and A. A. Chughtai, "Facemasks for the prevention of infection in healthcare and community settings," *BMJ*, vol. 350, p. 694, Apr. 2015, doi: 10.1136/bmj.h694.

[6] J. Howard et al., "An evidence review of face masks against COVID-19," *Proc. Nat. Acad. Sci. USA*, vol. 118, no. 4, Jan. 2021, Art. no. e2014564118, doi: 10.1073/pnas.2014564118.

[7] K. L. Andrejko, "Effectiveness of face mask or respirator use in indoor public settings for prevention of SARS-CoV-2 infection—California, February-December 2021," *MMWR Morb Mortal Wkly Rep.*, vol. 71, no. 6, pp. 212–216, 2022, doi: 10.15585/mmwr.mm7106e1.

[8] (Aug. 20, 2021). *Order: Wearing of Face Masks While on Conveyances and at Transportation Hubs | Quarantine | CDC*. Accessed: Nov. 29, 2021. [Online]. Available: https://www.cdc.gov/quarantine/masks/mask-travel-guidance.html

[9] *When and How to Use Masks*. Accessed: Nov. 29, 2021. [Online]. Available: https://www.who.int/emergencies/diseases/novel-coronavirus-2019/advice-for-public/when-and-how-to-use-masks

[10] D. L. Rondinone et al., "Challenges in the supply chain for personal protective equipment (PPE) during COVID-19," *J. Text. Appar. Technol. Manag.*, vol. 12, pp. 1–23, Mar. 2021, Accessed: Nov. 15, 2021. [Online]. Available: https://ojs.cnr.ncsu.edu/index.php/JTATM/article/view/18052

[11] F. Tessarolo et al., "Testing surgical face masks in an emergency context: The experience of Italian laboratories during the COVID-19 pandemic crisis," *Int. J. Environ. Res. Public Health*, vol. 18, no. 4, p. 1462, Feb. 2021, doi: 10.3390/ijerph18041462.

[12] B. Krishan, D. Gupta, G. Vadlamudi, S. Sharma, D. Chakravortty, and S. Basu, "Efficacy of homemade face masks against human coughs: Insights on penetration, atomization, and aerosolization of cough droplets," *Phys. Fluids*, vol. 33, no. 9, Sep. 2021, Art. no. 093309, doi: 10.1063/5.0061007.

[13] W. Hao, G. Xu, and Y. Wang, "Factors influencing the filtration performance of homemade face masks," *J. Occupational Environ. Hygiene*, vol. 18, no. 3, pp. 128–138, Mar. 2021, doi: 10.1080/15459624.2020.1868482.

[14] European Committee for Standardisation. (Jun. 2020). *Workshop Agreement CWA 17553: 2020 E, Community Face Coverings—Guide to Minimum Requirements, Methods of Testing and Use*. Accessed: Aug. 30, 2021. [Online]. Available: https://www.cencenelec.eu/research/CWA/Documents/CWA17553_2020.pdf

[15] World Health Organization. (Jan. 2020). *Advice on the Use of Masks in the Community, During Home Care and in Health Care Settings in the Context of the Novel Coronavirus (2019-nCoV) Outbreak: Interim Guidance*. Accessed: Sep. 29, 2022. [Online]. Available: https://apps.who.int/iris/handle/10665/330987

[16] European Committee for Standardization. *Medical Face Masks—Requirements and Test Methods*, Standard 14683, 2019.

[17] (Jul. 1, 2019). *Standard Test Method for Evaluating the Bacterial Filtration Efficiency (BFE) of Medical Face Mask Materials, Using a Biological Aerosol of Staphylococcus Aureus-F2101–19*. ASTM International West Conshohocken, PA, USA. Accessed: Nov. 29, 2021. [Online]. Available: https://standards.globalspec.com/std/13404922/astm-f2101-19

[18] F23 Committee, *Standard Specification for Barrier Face Coverings*, ASTM International, West Conshohocken, PA, USA, doi: 10.1520/F3502-21.

[19] I. A. Carr et al., "In silico fit evaluation of additively manufactured face coverings," *Ann. Biomed. Eng.*, vol. 51, pp. 34–44, Jul. 2022, doi: 10.1007/s10439-022-03026-8.

[20] C. D. Cappa, S. Asadi, S. Barreda, A. S. Wexler, N. M. Bouvier, and W. D. Ristenpart, "Expiratory aerosol particle escape from surgical masks due to imperfect sealing," *Sci. Rep.*, vol. 11, no. 1, p. 12110, Jun. 2021, doi: 10.1038/s41598-021-91487-7.

[21] C. Freeman et al., "Do they really work? Quantifying fabric mask effectiveness to improve public health messaging," *Int. J. Environ. Res. Public Health*, vol. 19, no. 11, p. 6372, May 2022, doi: 10.3390/ijerph19116372.

[22] S. Verma, M. Dhanak, and J. Frankenfield, "Visualizing the effectiveness of face masks in obstructing respiratory jets," *Phys. Fluids*, vol. 32, no. 6, Jun. 2020, Art. no. 061708, doi: 10.1063/5.0016018.

[23] S. A. Grinshpun, H. Haruta, R. M. Eninger, T. Reponen, R. T. McKay, and S.-A. Lee, "Performance of an N95 filtering facepiece particulate respirator and a surgical mask during human breathing: Two pathways for particle penetration," *J. Occupational Environ. Hygiene*, vol. 6, no. 10, pp. 593–603, Sep. 2009, doi: 10.1080/15459620903120086.

[24] R. Mittal, R. Ni, and J.-H. Seo, "The flow physics of COVID-19," *J. Fluid Mech.*, vol. 894, p. F2, Jul. 2020, doi: 10.1017/jfm.2020.330.

[25] B. Y. H. Liu, J.-K. Lee, H. Mullins, and S. G. Danisch, "Respirator leak detection by ultrafine aerosols: A predictive model and experimental study," *Aerosol Sci. Technol.*, vol. 19, no. 1, pp. 15–26, Jan. 1993, doi: 10.1080/02786829308959617.

[26] Z. Lei, J. Yang, Z. Zhuang, and R. Raymond, "Simulation and evaluation of respirator faceseal leaks using computational fluid dynamics and infrared imaging," *Ann. Occupat. Hygiene*, vol. 57, no. 4, pp. 493–506, 2013, doi: 10.1093/annhyg/mes085.

[27] S. Chiera et al., "A simple method to quantify outward leakage of medical face masks and barrier face coverings: Implication for the overall filtration efficiency," *Int. J. Environ. Res. Public Health*, vol. 19, no. 6, p. 3548, Mar. 2022, doi: 10.3390/ijerph19063548.

[28] T. Solano, C. Ni, R. Mittal, and K. Shoele, "Perimeter leakage of face masks and its effect on the mask's efficacy," *Phys. Fluids*, vol. 34, no. 5, May 2022, Art. no. 051902, doi: 10.1063/5.0086320.

[29] M. A. Ortiz, M. Ghasemieshkaftaki, and P. M. Bluyssen, "Testing of outward leakage of different types of masks with a breathing manikin head, ultraviolet light and coloured water mist," *Intell. Build. Int.*, vol. 14, pp. 623–641, Sep. 2022, doi: 10.1080/17508975.2021.1951153.

[30] B. Ipaki, Z. Merrikhpour, M. S. T. Rizi, and S. Torkashvand, "A study on usability and design parameters in face mask: Concept design of UVW face mask for COVID-19 protection," *Hum. Factors Ergonom. Manuf. Service Industries*, vol. 31, no. 6, pp. 664–678, Nov. 2021, doi: 10.1002/hfm.20934.

[31] C. C. Chen and K. Willeke, "Aerosol penetration through surgical masks," *Am. J. Infect. Control*, vol. 20, no. 4, pp. 177–184, Aug. 1992, doi: 10.1016/s0196-6553(05)80143-9.

[32] A. Weber et al., "Aerosol penetration and leakage characteristics of masks used in the health care industry," *Am. J. Infect. Control*, vol. 21, no. 4, pp. 167–173, Aug. 1993, doi: 10.1016/0196-6553(93)90027-2.

[33] A. Balazy, M. Toivola, A. Adhikari, S. K. Sivasubramani, T. Reponen, and S. A. Grinshpun, "Do N95 respirators provide 95% protection level against airborne viruses, and how adequate are surgical masks?" *Amer. J. Infection Control*, vol. 34, no. 2, pp. 51–57, Mar. 2006, doi: 10.1016/j.ajic.2005.08.018.

[34] J. Pan, C. Harb, W. Leng, and L. C. Marr, "Inward and outward effectiveness of cloth masks, a surgical mask, and a face shield," *Aerosol Sci. Technol.*, vol. 55, no. 6, pp. 718–733, Jun. 2021, doi: 10.1080/02786826.2021.1890687.

[35] W. G. Lindsley et al., "A comparison of performance metrics for cloth face masks as source control devices for simulated cough and exhalation aerosols," *Aerosol Sci. Technol.*, vol. 55, no. 10, pp. 1125–1142, 2021, doi: 10.1101/2021.02.16.21251850.

[36] V. Arumuru, J. Pasa, and S. S. Samantaray, "Experimental visualization of sneezing and efficacy of face masks and shields," *Phys. Fluids*, vol. 32, no. 11, Nov. 2020, Art. no. 115129, doi: 10.1063/5.0030101.

[37] T.-K. Wang, T. Solano, and K. Shoele, "Bridge the gap: Correlate face mask leakage and facial features with 3D morphable face models," *J. Exposure Sci. Environ. Epidemiology*, vol. 32, no. 5, pp. 735–743, Sep. 2022, doi: 10.1038/s41370-021-00399-1.

[38] T. Solano, C. Ni, R. Mittal, and K. Shoele, "Perimeter leakage of face masks and its effect on the mask's efficacy," *Phys. Fluids*, vol. 34, no. 5, May 2022, Art. no. 051902, doi: 10.1063/5.0086320.

[39] Y.-J. Kwon, J.-G. Kim, and W. Lee, "A framework for effective face-mask contact modeling based on finite element analysis for custom design of a facial mask," *PLoS ONE*, vol. 17, no. 7, Jul. 2022, Art. no. e0270092, doi: 10.1371/journal.pone.0270092.

[40] L. H. Kwong et al., "Review of the breathability and filtration efficiency of common household materials for face masks," *ACS Nano*, vol. 15, no. 4, pp. 5904–5924, Apr. 2021, doi: 10.1021/acsnano.0c10146.

[41] J. Taborri, B. Stocchi, G. Calabro, and S. Rossi, "On the breathability measurement of surgical masks: Uncertainty, repeatability, and reproducibility analysis," *IEEE Trans. Instrum. Meas.*, vol. 71, pp. 1–9, 2022, doi: 10.1109/TIM.2022.3142754.

[42] F. Tessarolo et al., "Measuring breathability and bacterial filtration efficiency of face masks in the pandemic context: A round Robin study with proficiency testing among non-accredited laboratories," *Measurement*, vol. 189, Feb. 2022, Art. no. 110481, doi: 10.1016/j.measurement.2021.110481.
[43] S. Chiera et al., "The role of filter breathability in reducing the fraction of exhaled air leaking from surgical and community face masks," in *Proc. IEEE Int. Symp. Med. Meas. Appl. (MeMeA)*, Jun. 2022, pp. 1–6, doi: 10.1109/MeMeA54994.2022.9856516.
[44] S. Whitaker, "Flow in porous media I: A theoretical derivation of Darcy's law," *Transp. Porous Media*, vol. 1, no. 1, pp. 3–25, 1986, doi: 10.1007/BF01036523.
[45] J. T. Mueller, S. Karimi, K. A. Poterack, M. T. A. Seville, and S. M. Tipton, "Surgical mask covering of N95 filtering facepiece respirators: The risk of increased leakage," *Infection Control Hospital Epidemiol.*, vol. 42, no. 5, pp. 627–628, May 2021, doi: 10.1017/ice.2021.50.
[46] *Respiratory Protective Devices—Methods of Test and Test Equipment—Part 9: Determination of Carbon Dioxide Content of the Inhaled Gas*, Standard 16900-9:2015, Accessed: Dec. 19, 2022. [Online]. Available: https://standards.iteh.ai/catalog/standards/iso/ee264fed-dcd0-45e0-a594-06f9a7288e80/iso-16900-9-2015
[47] European Committee for Standardization. *Respiratory Protective Devices—Filtering Half Masks to Protect Against Particles—Requirements, Testing, Marking*, Standard EN 149:2001+A1, 2009.
[48] European Committee for Standardization. *European Respiratory Protective Devices—Filtering Half Masks to Protect Against Particles—Requirements, Testing, Marking*, Standard EN 149:2009+A1, 2009.
[49] J. K. Gupta, C. -H. Lin, and Q. Chen, "Characterizing exhaled airflow from breathing and talking," *Indoor Air*, vol. 20, pp. 31–39, Feb. 2010, doi: 10.1111/j.1600-0668.2009.00623.x.
[50] *GUM 1995 With Minor Corrections, Data—Guide to the Expression of Uncertainty in Measurement*, Joint Committee for Guides in Metrology, Standard JCGM 100, Sep. 2008.
[51] D. C. Montgomery, *Design and Analysis of Experiments*, 8th ed. Hoboken, NJ, USA: Wiley, 2013.
[52] D. C. Montgomery and V. M. Bettencourt, "Multiple response surface methods in computer simulation," *Simulation*, vol. 29, no. 4, pp. 113–121, Oct. 1977, doi: 10.1177/003754977702900406.
[53] M. A. Hadiyat, B. M. Sopha, and B. S. Wibowo, "Response surface methodology using observational data: A systematic literature review," *Appl. Sci.*, vol. 12, no. 20, p. 10663, Oct. 2022, doi: 10.3390/app122010663.
[54] *R: A Language and Environment for Statistical Computing. Reference Index. The R Development Core Team. Version 2.6.2*, R Found. Stat. Comput., Inst. Statist. Math., Vienna, Austria, Feb. 2008.
[55] A. Bucciarelli, S. Chiera, A. Quaranta, V. K. Yadavalli, A. Motta, and D. Maniglio, "A thermal-reflow-based low-temperature, high-pressure sintering of lyophilized silk fibroin for the fast fabrication of biosubstrates," *Adv. Funct. Mater.*, vol. 29, no. 42, Oct. 2019, Art. no. 1901134, doi: 10.1002/adfm.201901134.
[56] A. Bucciarelli, A. Adami, C. R. Chandaiahgari, and L. Lorenzelli, "Multivariable optimization of inkjet printing process of Ag nanoparticle ink on Kapton," in *Proc. IEEE Int. Conf. Flexible Printable Sensors Syst. (FLEPS)*, Aug. 2020, pp. 1–4, doi: 10.1109/FLEPS49123.2020.9239474.
[57] A. M. Bossi, A. Bucciarelli, and D. Maniglio, "Molecularly imprinted silk fibroin nanoparticles," *ACS Appl. Mater. Interfaces*, vol. 13, no. 27, pp. 31431–31439, Jul. 2021, doi: 10.1021/acsami.1c05405.
[58] R. Peric and M. Peric, "Analytical and numerical investigation of the airflow in face masks used for protection against COVID-19 virus—Implications for mask design and usage," *J. Appl. Fluid Mech.*, vol. 13, no. 6, pp. 1911–1923, Nov. 2020, doi: 10.47176/jafm.13.06.31812.
[59] S. Asadi, C. D. Cappa, S. Barreda, A. S. Wexler, N. M. Bouvier, and W. D. Ristenpart, "Efficacy of masks and face coverings in controlling outward aerosol particle emission from expiratory activities," *Sci. Rep.*, vol. 10, no. 1, pp. 1–13, Sep. 2020, doi: 10.1038/s41598-020-72798-7.
[60] S. Duncan, P. Bodurtha, and S. Naqvi, "The protective performance of reusable cloth face masks, disposable procedure masks, KN95 masks and N95 respirators: Filtration and total inward leakage," *PLoS ONE*, vol. 16, no. 10, Oct. 2021, Art. no. e0258191, doi: 10.1371/journal.pone.0258191.
[61] J. Xi, K. Barari, X. A. Si, M. Y. A. Jamalabadi, J. H. Park, and M. Rein, "Inspiratory leakage flow fraction for surgical masks with varying gaps and filter materials," *Phys. Fluids*, vol. 34, no. 4, Apr. 2022, Art. no. 041908, doi: 10.1063/5.0090356.
[62] T. Solano and K. Shoele, "Investigation of the role of face shape on the flow dynamics and effectiveness of face masks," *Fluids*, vol. 7, no. 6, p. 209, Jun. 2022, doi: 10.3390/fluids7060209.
[63] J. Taborri, B. Stocchi, G. Calabro, and S. Rossi, "Repeatability and reproducibility in the breathability measurement of surgical masks," in *Proc. IEEE Int. Symp. Med. Meas. Appl. (MeMeA)*, Jun. 2021, pp. 1–6, doi: 10.1109/MeMeA52024.2021.9478732.
[64] M. S. Bergman et al., "Development of an advanced respirator fit-test headform," *J. Occupational Environ. Hygiene*, vol. 11, no. 2, pp. 117–125, Feb. 2014, doi: 10.1080/15459624.2013.816434.

Silvia Chiera received the bachelor's degree in biomolecular sciences and technologies and the master's degree in cellular and molecular biotechnology from the University of Trento, Trento, Italy, in 2012 and 2015, respectively, and the Ph.D. degree in material, mechatronic, and system engineering from the Industrial Engineering Department, BIOTech Research Center, European Institute of Excellence on Tissue Engineering and Regenerative Medicine, University of Trento in 2021. Her Ph.D. thesis focused on anterior cruciate ligament tissue engineering and regeneration.

During her Ph.D., she collaborated with several research groups, including the Gilson Laboratory, Jeonbuk National University, Jeonju, South Korea, working on silk-based material in the context of the Research and Innovation Staff Exchange (RISE) Marie Curie Project (REMIX, https://r1.unitn.it/remix/) on tissue engineering, the Trauma Laboratory, Munich, Germany, and 3B's Research Group, Braga, Portugal. She is currently a Post-Doctoral Researcher with the University of Trento, where she focused on two main projects related to the identification of methods and tools for the characterization of technologies for the contrast of infectious agents (LASS-TN-Covid-19 Laboratory), and on regenerative strategies in dental implantology.

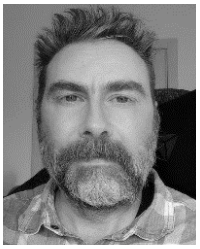

Alessandro Cristoforetti received the Laurea (M.S.) and Ph.D. degrees in physics from the University of Trento, Trento, Italy, in 2004 and 2009, respectively.

Since 2009, he has been a Researcher with the Laboratory of Biophysics and Biosignals, Department of Physics and the Department of Industrial Engineering, University of Trento. He collaborated to projects in the field of cardiac arrhythmias, interventional cardiology, diagnostic radiology, reconstructive dentistry, histology, robotic surgery, and health and safety science. His research interests include bio-signal processing, medical image processing, segmentation and registration of multimodal data, 3-D computer guided surgery, numerical methods for computational simulations, and medical prototyping and validation.

Luca Benedetti has been a Laboratory Technician with the Department of Industrial Engineering, University of Trento, Trento, Italy, since 1991. He works in the field of materials characterization and in particular in the study of the degradation and protection of materials and coatings through accelerated aging techniques and electrochemical tests. He gained a consolidated experience in the field of metallic and organic coatings for industrial use and biomaterials, in particular implantable prostheses, stents, and heart valves. Since March 2021, he has been a part of the LASS-TN-Covid-19, a Joined Laboratory between the University and the Provincial Heath Trust of Trento for testing safety and performance of personal protection devices and other technologies against SARS-CoV-2 virus.

Luca Borro was born in Velletri, Rome, Italy, in 1986. He received the degree in architecture sciences from the Sapienza University of Rome, Rome, in 2013, the degree in biological sciences from the University of Urbino "Carlo Bo," Urbino, Italy, in 2019, and the bachelor's degree in biomedical engineering from UNICUSANO, Rome, in 2021. He is currently pursuing the master's degree in health biology with the University of L'Aquila, L'Aquila, Italy.

Since 2015, he has been working as a Technical Manager with the 3D Laboratory, Bambino Gesù Children's Hospital, Rome, where he is responsible for 3-D design for biomedical applications, 3-D printing of patient-specific anatomical parts for preoperative planning in surgery, and 3-D bioprinting for regenerative medicine. He has collaborated with several Italian and European scientific institutions on various research projects. He worked with the Santa Lucia Research Institute, Rome, on a project involving the in vitro construction of biological constructs for the study of amyotrophic lateral sclerosis using 3-D bioprinting. He also collaborated with the San Raffaele Institute, Milan, Italy, on a project involving the study of pancreatic beta cells using 3-D printing and bioprinting. He has authored or coauthored several publications in scientific journals and conference proceedings. His previous research interests included the development of nanocomposite scaffolds for tissue engineering.

Lorenzo Mazzei was born in Prato, Italy, in 1987. He received the bachelor's degree in mechanical engineering, the master's degree in energy and nuclear engineering, and the Ph.D. degree in industrial engineering from the University of Florence, Florence, Italy, in 2009, 2011, and 2015, respectively. His Ph.D. thesis focused on computational fluid dynamics (CFD) methodologies for the estimation of thermal loads in gas turbine combustors.

He continued the academic experience at the University of Florence, as a Post-Doctoral Researcher until the end of 2018 and as an Adjunct Assistant Professor at the University of Florence, since 2019, supporting the activities in the master course "Gas Turbine Power Plants," where he teaches CFD for heat transfer applications. Since 2017, he has been working with Ergon Research, Florence, former spin-off of the University of Florence devoted to the technology transfer to the industry. He has authored more than 55 conference papers and more than 35 journal articles, mostly in the fields of gas turbine combustion and heat transfer, thermal management, and fluid dynamics.

Dr. Mazzei is an ASME Member and contributes constantly to the activities of the ASME IGTI K-14 Gas Turbine Heat Transfer Committee, and an Associate Editor of the *Journal of Turbomachinery* and a Session Organizer of the ASME Turbo Expo conferences.

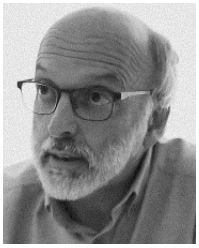

Giandomenico Nollo is currently an Associate Professor of Bioengineering with the Department of Industrial Engineering, University of Trento, Trento, Italy. He has conceived and led numerous national and international research projects aimed at the development and application of advanced health technologies, in collaboration with academia, industries, and health facilities. The analysis of biological signals for the modeling of the interaction processes between physiological systems, digital health, and the characterization of interface processes between implantable medical devices and tissues, functional performance, and safety of medical devices are the principal items of his research. He has authored over 220 scientific publications (HI-Scopus: 40).

Mr. Nollo served as a member of the Scientific Committee and the president of national and international workshops and conferences. He is currently the Deputy Vice-President of the Italian Society of Health Technology Assessment (SIHTA).

Alessio Bucciarelli received the M.Sc. degree in material science from the University of Venice, Venice, Italy, in 2013, and the Ph.D. degree in material, mechatronic, and system engineering from the Industrial Engineering Department, BIOTech Research Center, European Institute of Excellence on Tissue Engineering and Regenerative Medicine, University of Trento, Trento, Italy, in 2019.

During his Ph.D., he collaborated with several research groups, including the Bio-Nano Laboratory, Virginia Commonwealth University, Richmond, VA, USA, working on silk-based photoresist, and the Gilson Laboratory, Jeonbuk National University, Jeonju, South Korea, working on silk-based photoresin in the context of the Research and Innovation Staff Exchange (RISE) Marie Curie Project (REMIX, https://r1.unitn.it/remix/) on tissue engineering. In 2019, he joined the Microsystem Technology Group, Fondazione Bruno Kessler (FBK), Trento, to work on an industrial project within the Italian Polygraphic Institute and State Mint, Rome, Italy, working on inkjet and aerosol processes for the development of conductive layers. In FBK, he was the Main Instructor of a Ph.D. level course in design of experiment for the optimization of processes. He worked with the National Italian Council of Research (CNR-Nanotec), Lecce, Italy, to work in the development of photocrosslinkable biopolymer based bioinks and the process development of 3-D printed organ-on-chips devices. He is currently working with the Rizzoli Orthopedic Institute, Bologna, Italy. His research interests are mainly related to the use of statistical methods to optimize and standardize processes in the biomedical field.

Francesco Tessarolo the master's degree in biomaterials, and the Ph.D. degree in materials engineering from the University of Trento, Trento, Italy, in 2002, 2005, and 2006, respectively.

From 2006 to 2009 and from 2009 to 2013, he was a Post-Doctoral Research Fellow with the Department of Physics and the Biotech Center in Biomedical Technologies, University of Trento, respectively, having the role of Co-Investigator or Principal Investigator in several biomedical applied research projects and clinical investigations. He then moved to Bruno Kessler Foundation, Trento, for six years, joining the Healthcare Research and Innovation Program and participating in H2020 EU projects on radically new technologies to help older adults living independently at home. Since 2019, he has been with the Department of Industrial Engineering, University of Trento, where he currently holds a researcher position focused on innovative technologies for the multisensors real-time monitoring of processes and services in health care. Since March 2021, he has been technical responsible for the LASS-TN-Covid-19, a Joined Laboratory between the University and the Provincial Heath Trust of Trento for testing safety and performance of personal protection devices and other technologies against SARS-CoV-2 virus. He has authored more than 70 journal articles on peer-reviewed journal and more than 180 contributions at national and international conferences. His main research interests cover the fields of biomaterials and materials for medical applications, microbial biofilm and device-related infections, disinfection and sterilization, and information and communication technologies for the healthcare and wellbeing.

Open Access funding provided by 'Università degli Studi di Trento' within the CRUI CARE Agreement